The effect of increasing the horizontal resolution on the d~~D~~eep water formation in the North Atlantic Ocean in HighResMIP models ~~in high resolution global coupled climate models~~

Torben Koenigk[1,2], Ramon Fuentes-Franco[1], Virna L. Meccia[3], Oliver Gutjahr[4], Laura C. Jackson[5], Adrian L. New[6], Pablo Ortega[7], Christopher Roberts[8], Malcolm Roberts[5], Thomas Arsouze[7], Doroteaciro Iovino[9], Marie-Pierre Moine[10], Dmitry V. Sein[11]

[1] Rossby Centre, Swedish Meteorological and Hydrological Institute, Norrköping, Sweden
[2] Bolin Centre for Climate Research, Stockholm University, Sweden
[3] Istituto di Scienze dell'Atmosfera e del Clima (CNR-ISAC), Bologna, Italy
[4] Max Planck Institute for Meteorology, Hamburg, Germany
[5] Met Office, Exeter EX1 3PB, U.K
[6] The National Oceanography Centre Southampton, U.K.
[7] Barcelona Supercomputing Center – Centro Nacional de Supercomputación (BSC), Barcelona, Spain
[8] European Centre for Medium-Range Weather Forecasts (ECMWF), Reading, U.K
[9] Fondazione Centro Euro-Mediterraneo sui Cambiamenti Climatici (CMCC), Bologna, Italy
[10] CERFACS/CNRS, Toulouse, France
[11] Alfred Wegener Institute for Polar and Marine Research, Bremerhaven, Germany

Correspondence to: Torben Koenigk (torben.koenigk@smhi.se)

Abstract. Simulations from seven global coupled climate models performed at high and standard resolution as part of the High Resolution Model Intercomparison Project (HighResMIP) have been analyzed to study the impact of horizontal resolution in both ocean and atmosphere on deep ocean convection in the North Atlantic and to evaluate the robustness of the signal across models. The representation of convection varies strongly among models. Compared to observations from ARGO-floats, most models substantially overestimate deep water formation in the Labrador Sea. In the Greenland-Norwegian-Iceland (GIN) Seas, some models overestimate convection while others show too weak convection.

In four out of five ~~most~~ models with increased ocean resolution, higher ocean resolution leads to increased deep convection in the Labrador Sea. The effect of resolution on~~and reduced~~ convection in the ~~Greenland Sea~~GIN Seas is less clear. Increasing the atmospheric resolution has a smaller~~only little~~ effect on the deep convection than increasing the ocean resolution~~, except in two models, which share the same atmospheric component and show reduced convection~~. Simulated convection in the Labrador Sea is largely governed by the release of heat from the ocean to the atmosphere. Higher resolution models show stronger surface heat fluxes than the standard resolution models in the convection areas, which promotes the stronger convection in the Labrador Sea. In the GIN~~reenland~~ Seas, the connection between high resolution and ocean heat release to the atmosphere is less robust and there is more variation across models in the relation between surface heat fluxes and convection. Simulated freshwater fluxes have less impact than surface heat fluxes on convection in both the GIN~~reenland~~ and Labrador Seas and this result is insensitive to model resolution~~. is not robust across models~~. The mean strength of the Labrador Sea convection is important for the mean Atlantic Meridional Overturning Circulation (AMOC) and in around half of the models the variability of Labrador Sea convection is a significant contributor to the variability of the AMOC.

1 Introduction

Open-ocean deep convection is a rare phenomenon, occurring only at a few locations in the world's ocean. It provides a vertical link between properties of the surface ocean and the deep ocean. In the North Atlantic, the northward flowing warm water masses become denser because of large heat loss to the atmosphere and sink into the deep ocean. Deep convection ventilates the deep ocean with oxygen and plays an important role for the storage of carbon and heat.

The main convection sites in the North Atlantic are the Labrador and Irminger Seas as well as the Greenland-Iceland-Norwegian (GIN) Seas. Deep convection in the Labrador and Irminger Seas produces the deep water masses called Labrador Sea Water (LSW) (Clarke and Gascard, 1983), which together with the dense overflow waters coming through the Faroe Bank Channel and Denmark Strait (Dickson and Brown, 1994) form the North Atlantic Deep Water.

The deep convection in the Labrador Sea is mainly driven by wintertime buoyancy loss to the atmosphere (Latif et al., 2006; Frankignoul et al., 2009), which is strongly governed by the North Atlantic Oscillation (NAO). Also freshwater transports through Fram Strait contribute to the variability of deep convection in the Labrador Sea (Holland et al., 2001; Jungclaus et al., 2005; Koenigk et al., 2006). Labrador Sea convection varies strongly on interannual to decadal time scales (Yashayaev and Loder, 2016) and was rather shallow in the 1990s and 2000s, but recovered in recent years with mixing depths exceeding 2000m (Yashayaev and Loder, 2017). Convection in the GIN Seas occurred frequently down to the bottom until the 1980s. However, thereafter, no regularly occurring deep convection has been observed any more; between 1994 and 2002 mixing depths of 700-1600m have been monitored (Ronski and Budeus, 2005). Irminger Sea convection is generally weaker than in the Labrador and GIN Seas but in recent years mixing depth reached below 1000m depth (de Jong and de Steur, 2016; de Jong et al., 2018).

Variability and change of deep convection affects local and remote climate. Reduced convection in the Labrador Sea is linked to surface salinity, temperature and sea ice in Labrador Sea and Davis Strait (Deser et al. 2002) but has also remote effects on the atmospheric circulation (Koenigk et al. 2006). The deep convection has for long time been seen as the driving mechanism for the Atlantic Meridional Overturning Circulation (AMOC), which is fundamentally important for the climate in the North Atlantic and adjacent regions such as Western Europe and the Arctic (Manabe and Stouffer 1999; Mahajan et al., 2011, Koenigk et al., 2012; Jackson et al., 2015). However, more recently, the importance of deep convection for the AMOC has been questioned (Sayol et al., 2019). Kuhlbrodt et al. (2007) and Medhaug and Furevik (2011) identified wind-driven upwelling, gyre circulation, and wind and tidal vertical mixing as important processes sustaining the long-term strength of the AMOC, thus, a collapse of the deep convection would not necessarily lead to collapse of the AMOC (Gelderloos et al. 2012; Marotzke and Scott 1999). On the other hand, surface buoyancy forcing exerts a very strong control on exactly where and when the overturning occurs. Thus, even if mixing ultimately sets the strength of the global overturning, the deep water formation in the North Atlantic will play a key role in the strength of AMOC on decadal timescales.

Formaterat: Teckenfärg: Svart, Kerning från 16 pt

Many studies have discussed the potential for a weakening AMOC as a response to global warming (Cheng et al., 2013; Swingedouw et al., 2007; Brodeau and Koenigk, 2016; Koenigk and Brodeau, 2017) and linked the weakening to a reduction of the deep water formation (Latif et al., 2006; Deshayes et al., 2007; Koenigk et al., 2007; Frankignoul et al., 2009; Langehaug et al. 2012). Recent studies indicate an ongoing weakening of the AMOC at 26.5°N (Smeed et al. 2014; Smeed et al. 2018; Thornalley et al., 2018; Caesar et al., 2018) although it is unclear if this observed weakening is caused by climate change or internal decadal variability (e.g. Jackson et al., 2016; Roberts et al., 2014; Robson et al. 2016). Observational evidence for a link between dense water formation in the Labrador Sea and AMOC is still missing (Lozier et al. 2017, Lozier et al. 2019) but short observation period and potential lags of several years between AMOC and convection (Brodeau and Koenigk, 2016; Roberts et al. 2013) make robust conclusions from observations difficult.

The deep convective process is temporally intermittent and spatially compact. This makes it difficult to observe this process, and state-of-the-art climate models, such as CMIP6, need to use parameterizations to represent convective processes (Fox-Kemper et al., 2019). Given the importance of the deep convection for climate and its future change, a reliable representation in climate models is highly important. However, Heuzé (2017) stated that "the majority of CMIP5 models convect too deeply, over too large an area, too often and too far south". While CMIP6 models seem to provide some improvements in the representation of bottom waters, more improvements are required (Heuzé 2020).

Formaterat: Nivå 1, Håll ihop med nästa

Going beyond the horizontal resolution of CMIP6 models, we analyse in this study whether high-resolution models from the CMIP6 High-Resolution Model Intercomparison Project (HighResMIP, Haarsma et al., 2016) improve the representation of deep convection in the subpolar North Atlantic. We use simulations from seven models participating in HighResMIP, which have been performed in the EU-H2020-project PRIMAVERA. Most of the high-resolution model versions of these seven models have ocean grid resolutions of around 10-25 km. Since the baroclinic Rossby radius of deformation is small in high latitudes (roughly 10 km in polar regions and 200 km in the tropics), mesoscale oceanic eddies are not resolved in the sub-polar convection regions in most of the HighResMIP models. We thus denote them as "eddy permitting" but not "eddy-resolving".

Recent studies found that the increased resolution in the HighResMIP models improved many aspects of the ocean including temperature and salinity biases (Gutjahr et al. 2019), the northward ocean heat transport (Grist et al., 2019), sea ice in the Atlantic sector of the Arctic Ocean (Docquier et al., 2019; Docquier et al., 2020), the position of the North Atlantic Current (Chassignet and Marshall, 2008; Sein et al., 2018) as well as Arctic freshwater exports (Fuentes Franco and Koenigk, 2019).

After this introduction, we proceed with describing the models, the data and the methods in section 2. Sections 3 to 5 will show the results from this study and we will conclude in section 6.

The Atlantic Meridional Overturning Circulation (AMOC) is one important part of the global thermohaline circulation and transports heat in the upper ocean far to the north into the northern North Atlantic, and cold water masses to the south in the deep ocean.

Many studies have discussed the potential for a weakening and even collapse of the Atlantic Meridional Overturning Circulation (AMOC) as a response to global warming (Cheng et al., 2013; Swingedouw et al., 2007; Brodeau and Koenigk, 2016; Koenigk and Brodeau, 2017). Several recent studies further suggest that the AMOC has already reduced substantially compared to the preindustrial period. For example, Thornalley et al. (2018) used paleoclimatic reconstructions to show that the AMOC in the last 150 years was lower than at any other time in the last 1600 years. Caesar et al. (2018) used a fingerprint of the AMOC on sea surface temperature (SST) as an index for the AMOC and they found that this AMOC index showed the lowest values in the last few years since 1850. A reduction of the AMOC would have fundamental impacts on the climate in the North Atlantic region but also in adjacent regions such as Western Europe (Manabe and Stouffer 1999), the Arctic (Mahajan et al., 2011, Koenigk et al., 2012) and even for the large scale atmospheric circulation (Jackson et al., 2015). Direct observations from the RAPID array indicate an ongoing weakening of the AMOC at 26.5°N (Smeed et al. 2014; Smeed et al. 2018). However, the observational time period is short and it is difficult to know whether or not this weakening is part of a long term response to climate change or part of internal decadal variability (e.g. Jackson et al., 2016; Roberts et al., 2014; Robson et al. 2016).

Deep convection is a key oceanic process that ventilates the lower limb of the AMOC, and contributes to the storage of heat, anthropogenic carbon and oxygen in the deep ocean. Although the idea that deep convection is accompanied by large amounts of sinking water and that this deep water formation is the main mechanism for driving the AMOC has been questioned (Sayol et al., 2019), a reduction of deep wintertime convective mixing in the northern North Atlantic will likely have important impacts for the AMOC. Without the deep mixing, less North Atlantic Deep Water (NADW) is formed (Dickson and Brown, 1994). Kuhlbrodt et al. (2007) and Medhaug and Furevik (2011) identified wind driven upwelling, gyre circulation, and wind and tidal vertical mixing as important processes sustaining the long term strength of the AMOC, and a potential collapse of deep water convection in the North Atlantic would not necessarily lead to a collapse of the AMOC (Marotzke and Scott, 1999; Kuhlbrodt et al., 2007; Gelderloos et al., 2012). On the other hand, surface buoyancy forcing exerts a very strong control on exactly where and when the overturning occurs. Thus, even if mixing ultimately sets the strength of the global overturning, the deep water formation in the North Atlantic will play a key role in the strength of AMOC on decadal timescales. In many future model simulations, deep convection in the North Atlantic declines rapidly due to surface warming and freshening (Latif et al., 2006; Deshayes et al., 2007; Koenigk et al., 2007; Frankignoul et al., 2009) but the AMOC shows a comparatively smaller reduction of 5-40% depending on model and emission scenario (Cheng, 2013). However, these studies still show the importance of deep water formation for the amplitude and variability of the AMOC (Lozier et al. 2019).

The question whether and to what extent deep water formation in the Labrador Sea is a driver for the AMOC and its variability is still discussed. While many modelling studies (Jungclaus et al., 2005; Kuhlbrodt et al., 2007; Gelderloos et al.,

2012; Eden and Willebrand, 2001; Biastoch et al., 2008; Brodeau and Koenigk, 2016; Ba et al., 2014; Roberts et al., 2013) showed a high correlation between the Labrador Sea convection and the variability of the AMOC at different time scales, no conclusive observational evidence for a link between dense water formation in the Labrador Sea and AMOC variability has emerged to date (Lozier et al. 2017, Lozier et al. 2019). The short observation period, however, might make it difficult to draw robust conclusions on the link between Labrador Sea convection and AMOC since model simulations suggest that the AMOC lags the Labrador Sea convection by several years (Brodeau and Koenigk, 2016; Roberts et al. 2013).

The deep convection in the Labrador Sea is mainly driven by wintertime buoyancy loss to the atmosphere (Latif et al., 2006; Frankignoul et al., 2009). The buoyancy loss itself is strongly governed by the North Atlantic Oscillation (NAO); during a positive NAO, cold air is advected from the Arctic southward over the sea ice to the Labrador Sea and leading to large buoyancy loss to the atmosphere and consequently strong convective mixing in the Labrador Sea. Labrador Sea convection varies strongly on interannual to decadal time scales (Yashayaev and Loder, 2016). While the convection was rather shallow since the early 1990s, the period 2012-2016 was one of the most persistent periods with Labrador Sea convective activity ever observed since 1938 (although observations were scarce over most of the 20th century), and the winter of 2016 showed a widespread convective activity down to 2200m (Yashayaev and Loder, 2017). Irminger Sea convection was also strong in recent years and reached record levels in the winter 2014/ 2015 (de Jong and de Steur, 2016; de Jong et al., 2018). The transport of freshwater from the Fram Strait along the Greenland coast into the Labrador Sea is another contributing factor, with increased freshwater fluxes leading to reduced salinities that suppress deep convection in the Labrador Sea (Holland et al., 2001; Jungclaus et al., 2005; Koenigk et al., 2006).

Deep convection in the Nordic Seas may also play an important role (Lozier et al., 2019). Langehaug et al. (2012) linked the variability of the AMOC to the variability of the overflows across the Greenland-Scotland Ridge.

Because of the coupled nature of the involved processes, coupled climate models are in principle well suited to study the interactions between deep convection and other climate related processes. However, Heuze (2017) stated that "the majority of CMIP5 models convect too deeply, over too large an area, too often and too far south". Further, Heuze (2017) found that deep convection is best simulated in those models with realistic ice edges in the North Atlantic.

In this study, we analyze the impact of increasing the horizontal resolution on the deep convection in the North Atlantic. We use simulations from seven models participating in the High Resolution Model Intercomparison Project (HighResMIP, Haarsma et al., 2016), which have been performed in the EU-H2020 project PRIMAVERA. High resolution has been shown to improve many aspects of the ocean circulation. Gutjahr et al. (2019) showed a reduction of temperature and salinity biases in the MPI-ESM1-2 model with eddy resolving ocean resolution. Grist et al. (2018) showed a more realistic northward ocean heat transport in high resolution models that results consequently in a more realistic representation of the sea ice in the Atlantic sector of the Arctic Ocean (Docquier et al., 2019). High resolution ocean models also substantially improve the position of the North Atlantic Current (Chassignet and Marshall, 2008; Sein et al., 2018). Furthermore, higher horizontal resolution might lead to a more realistic simulation of freshwater exports out of the Arctic (Fuentes-Franco and Koenigk, 2019) and a better representation of the properties and position of the dense overflows.

~~After this introduction, we proceed with describing the models, the data and the methods in section 2. Sections 3 to 5 will show the results from this study and we will conclude in section 6.~~

2 Models, data and method

2.1 Models and simulations

In this study we analyze seven global coupled climate models (see e.g. Vannière et al., 2019), which participated in the HighResMIP experiment (Haarsma et al. 2016) within the H2020-EU-project PRIMAVERA. These models are ECMWF-IFS (Roberts et al., 2018), HadGEM3-GC31 (Roberts et al., 2019), MPI-ESM1.2 (Gutjahr et al,. 2019), CMCC-CM2 (Cherchi et al., 2019), CNRM-CM6.1 (Voldoire et al., 2019), AWI-CM-1.0 (Sidorenko et al., 2014, HR and LR setups: Sein et al., 2016) and EC-Earth3P (Haarsma et al., 2020). The set of HighResMIP experiments is divided into three tiers consisting of atmosphere-only and coupled runs and spanning the period 1950-2050 (details in Haarsma et al. 2016). Here, w~~W~~e use the Tier 2 historical coupled simulations from 1950-2014 and the 100-year control simulations ~~(using constant 1950 forcing)~~ from these seven models for our analysis. The control run used fixed 1950s forcing (GHG gases, including O3 and aerosol loading for a 1950s (~10 year mean) climatology). They will allow to evaluate potential model drifts in the historical simulations. Both control and historical runs are initialized from the end of 50 year spin-up simulations using 1950s-forcing. All models performed historical and control~~the~~ simulations in at least two different resolutions. ~~following the HighResMIP protocol.~~ Changes in oceanic and atmospheric parameters are kept to a minimum between low and high resolution simulations, so that all changes can be directly attributed to the change in resolution.

The resolution varies among models. A few of the models vary both ocean and atmosphere resolution at the same time while others separately changed ocean or atmosphere resolution. This allows us to analyze also the effect of increasing the resolution in only one component of the system. Five of the seven models use the NEMO-ocean model as ocean component. While this might limit the robustness of our conclusions across models, it has to be noted that the NEMO-model configurations differ quite substantially from each other with different sea ice models (LIM2, LIM3, GELATO, CICE) and differences in parameters (e.g. Gent McWilliams versus Smagorinsky). AWI-CM-1-0 and MPI-ESM1.2 use the same atmosphere component but different ocean components.

More details on the models and the simulations used in this study are provided in table 1.

2.2 Observational data

To compare the mixed layer depth (MLD) from the models to observations, the typical variable used to represent ocean convection depth, we use data from ARGO-profiles (Holte et al. 2017) provided on a 1° grid. In the ARGO-data, the de Boyer Montégut et al. (2004) variable density threshold (0.03 kg m^{-3}) is used to calculate the mixed layer depth. Two different ARGO data sets of the mixed layer depth are used in this study: first, the climatological mean MLD in each grid point in March in the years 2000-2015; second, the maximum (mean over the two largest observed values in the period

Formaterat: Upphöjd

2000-2015) MLD in each grid-point. Note that in many grid-points only a few ARGO-profiles exist and in some no profiles at all. Further, ARGO-floats generally sample to a depth of 2000m, thus MLD extending below 2000m are not captured. In addition, the observational time period is short given the long time scales of variability in deep water formation. Thus, the ARGO-observations do only provide an estimate of the observed MLD.

We use turbulent latent and sensible heat fluxes from the global ocean-surface heat flux products (1958-2006) developed by the Objectively Analyzed air-sea Heat Fluxes project at the Woods Hole Oceanographic Institution (WHOI-OAFlux) to evaluate the surface heat fluxes in our models. We use monthly means of the WHOI-OAFlux data on a 1° grid from 1958 onwards.

2.3 Method

Several different indices have been defined for the deep convection in the ocean (e.g. Schott et al., 2009; Yashayaev and Loder, 2009; Lavergne et al., 2014; Koenigk et al., 2007; L'Heveder et al., 2012). These indices take into account either the maximum MLD~~deepest reaching convection~~ and/ or the horizontal extent of the MLD. However, none of them excludes convective events that are too shallow to contribute to deep water formation. To overcome this problem, Brodeau and Koenigk (2016) defined the so-called "Deep Mixed Volume" (DMV) index, which only considers the convective mixing below a specific depth (critical depth z_{crit}) and integrates the volume of these deep mixed water masses in different convection regions of the North Atlantic. In our study, we use the DMV index for monitoring the deep convection~~. Following Brodeau and Koenigk (2016), we use~~ using a critical depth of 1000m for the Labrador Sea and 700m for the ~~Greenland Sea~~GIN Seas (Brodeau and Koenigk, 2016). In the Labrador Sea, convection must~~needs to~~ reach a depth of around 1000m in order to~~to be able to sustain the~~ renew~~wal of~~ the Labrador Sea water and contribute to the~~eventually become~~ North Atlantic Deep Water (Yashayaev, 2007). In the Nordic Seas, convection needs to at least reach down to the sill depth of the Denmark Strait and Faroe Bank Channel, which is around 600-700m in the models. We define the Labrador Sea region as 70° W - 40° W, 45° N - 72° N and the ~~Greenland Sea~~GIN Seas region as 20° W - 20° E, 65° N - 82° N. The main areas of Labrador and ~~Greenland Sea~~GIN ~~s~~Seas convection in all models fall into these regions.~~regions.~~ Although intermittent deep convection can occur in the Irminger Sea as well, we focus here only on the two regions with deepest convection. As will be shown in the results sections, none of the models show any substantial deep convection in the Irminger Sea. ~~.~~

We use monthly mean values of the March MLD of the model simulations to calculate the DMV. Note, that short convection episodes that exceed z_{crit} might thus be missed. The ocean mixed layer thickness in the models (variable mlotst following CMIP6-convections) is defined by the depth at which a change from the surface sigma-t of 0.125 has occurred (sigma-t criterion, Levitus, 1982). Note, that this definition differs slightly from the one used in the ARGO-data.

We also calculate the DMV from the ARGO data as comparison to the model results. We infilled grid-points with missing data in the ARGO-data by interpolating the nearest neighbours. This and the short time series of the ARGO-data lead to uncertainties in the calculations of the DMV from ARGO and therefore it only provides a rough estimate for the real world.

Formaterat: Teckensnitt:Inte Kursi

As an additional comparison, we also calculate the DMV based on critical depths of 0m, thus considering the full mixed layer.

For correlations, we calculate the Pearson correlation coefficient (r). We call a correlation significantly different from 0, if the p-value of the Pearson correlation coefficient is 0.05 or smaller based on a two-sided student-t distribution. Assuming 98 (N-2) degrees of freedom (assuming independence of each year of data in the 100-year (N=100) 1950-control simulations), the correlation is significant if |r| exceeds 0.2. When taking the autocorrelation of the variables into account, the degrees of freedom are reduced and differ depending on model and variable.

For calculation of the power spectrum, we used the method of Torrence and Compo (1998). Fourier transforms are calculated and red noise is used as background spectrum. To determine significance levels for the Fourier spectra the method of Torrence and Compo (1998) assumes that different realizations of the geophysical process will be randomly distributed about this background spectrum, and the actual spectrum can be compared against this random distribution.

Formaterat: Teckensnitt:Inte Kursi

3 Deep Convection in the North Atlantic

This section analyzes first the MLD in March, the month with the strongest convection in both observations and models, in the North Atlantic in the different models and in ARGO. Then, we focus on the DMV in the models, its variability and potential trends in the historical simulations.

3.1 Mixed layer depth

Figure 1 shows the averaged March MLD from ARGO and from all historical model simulations. In the period 2000-2015, the ARGO data suggest average MLDs of about 1000 m in the Labrador and ~~Greenland Sea~~GIN ~~s~~Seas. In the models, the MLD differs greatly and shows a strong dependence on the spatial resolution. While ECMWF-IFS-LR and EC-Earth3P show no or very shallow MLD in the main convection areas of the North Atlantic, many of the other simulations strongly overestimate the MLD compared to ARGO. Some models simulate much too strong convection in the Labrador Sea but do not show any deep convection in the ~~Greenland Sea~~GIN Seas while other models overestimate the MLD in both seas. In contrast, in the Irminger Sea, the MLD is more consistent across models and agrees better with ARGO. Note that we here compare models' MLD averaged over 1950-2014 with ARGO-data from 2000-2015. As we will discuss later more in detail, some of the models show a weakening of the convection with time, particularly in the Labrador Sea. ~~Thus comparing the same time period in models and ARGO would slightly reduce the overestimation of MLD compared to ARGO in these models.~~

Although the convection centre varies somewhat across models, we do not find any clear linkage to resolution. The models with particularly deep mixed layers show also the largest convection areas. Thus, compared to ARGO, they do not only overestimate the depth of mixed layer but also the area of deep convection.

The MLD deepens with increasing ocean resolution in all models, except for AWI-CM-1-0. However, the models showing deepening MLDs are not fully independent, because they share NEMO as the ocean component, whereas AWI-CM-1-0 has FESOM as ocean component. On the other hand, even the ~~global~~ models with NEMO3.6 as ocean component (compare HadGEM3-GC31, CNRM-CM6.1, CMCC-CM2 and EC-Earth3P) differ considerably. This discrepancy suggests that either the different atmospheric components or the choice of ocean parameters have a strong influence on the convection.

In contrast, the MLD differs little when the atmosphere resolution is increased ~~Differences in MLD between model versions where only the atmospheric resolution is increased are small compared to the effect of increased ocean resolution~~ (compare ECMWF-IFS-MR and ECMWF-IFS-HR, HadGEM3-GC31-MM with HadGEM3-GC31-HM, CCCM-CM2-HR4 with CCCM-CM2-VHR4). An exception is ~~for the~~ MPI-ESM1-2, where an increased atmospheric resolution ~~leads to~~ reduces~~d~~ MLD. This MLD reduction can ~~likely~~ be linked to too weak wind forcing in MPI-ESM1-2-XR (Putrasahan et al., 2019).

To investigate the impact of natural variability on the mean March MLD in the historical period and to quantify~~verify~~ the potential contribution of natural variations to the differences in MLD with changing resolution, we use an ensemble of historical simulations with the ECMWF-IFS model. The MLD in the low resolution version ECMWF-IFS-LR is very shallow in all 6 ensemble members and there is no deep convection in the historical and control simulations (not shown). Thus, we concentrate in the following on the four members of ECMWF-IFS-HR, which all exhibit pronounced deep mixing, particularly in the Labrador Sea. These four ECMWF-IFS-HR members underlie~~indicate~~ a considerable natural variability (Figure 2 a-d). The averaged March MLD (1950-2014) deviates in individual ensemble members up to about 200m from the ensemble mean MLD. Although, this is a considerable amount, given the relatively long averaging period, the MLD differences due to increased resolution from 1° to a 0.25° in the NEMO-models are larger (compare Figure 2 to differences between 1° and 0.25° simulations in Figure 1). ~~Figure 2f shows the DMV in the Labrador Sea for the ensemble mean and the four ECMWF-IFS-HR members.~~ Although the DMV varies considerably between the ensemble member, the general amplitude, frequency and trends are similar.~~There is substantial spread across members but no generally different behavior in amplitude and time scales of variability and trends across model members can be seen.~~

Even though four members are not sufficient to capture the total natural variability, these results suggest that natural variability cannot explain the differences in MLD due to a change in spatial resolution.

3.2 Deep Mixed Volume

In the following, in order to consider the horizontal extension of convection patterns and discard shallow convection events that have limited impact on the oceanic circulation such as the AMOC, we will concentrate on the DMV index to investigate the deep convection in the Labrador and ~~Greenland Sea~~GIN ~~s~~Seas in more detail.

3.2.1 Labrador Sea

Figure 3 shows the DMV in the Labrador Sea in March in the historical model simulations. In agreement with Figure 1, increasing the ocean resolution from around 1° to 0.25° ~~in the ocean~~ generally leads to an increased DMV in all models using NEMO (ECMWF-IFS, HadGEM3-GC31, CNRM-CM6-1, EC-Earth3P, see Table 2.1), while the opposite is true for AWI-CM-1-0. I~~A further i~~ncreasing the~~e in~~ ocean resolution further to 1/12 ° in HadGEM3-GC31-HH does not further increase the DMV. The DMV varies strongly among models: ECMWF-IFS-LR does not show any deep convection events in the entire historical period, CNRM-CM6.1 and EC-Earth3P simulate only a few events with deep convection and AWI-CM-1-0-LR and CMCC-CM2 simulate strong deep convection every winter.

Table 2 compares the average DMV in the ~~-~~historical model simulations with that of ARGO in the period 2000-2015. We compare both the entire period 1950-2014 and the period 2000-2014 to ARGO. Generally, the simulated DMV in the Labrador Sea is smaller in 2000-2014 compared to the entire period. On the other hand, natural variability of the DMV is high and thus a 15-year period is probably too short for a comparison. ~~The only simulation that shows similar values in the Labrador Sea as ARGO is~~ The DMV in EC-Earth3P-HR and CNRM-CM6.1 are closest to ARGO when considering the entire 1950-2014 period into account, however, they underestimate ARGO in 2000-2014. As discussed above, EC-Earth3P and ECMWF-IFS-LR show no or rather little deep convection in the Labrador Sea while the other simulations ~~(except for CNRM-CM6.1)~~ overestimate the ARGO-based DMV with factors of four to almost 40 when taking the entire time period into account (3-25 in the period 2000-2014). The MPI-ESM1.2-XR overestimates ARGO in 1950-2014 but substantially underestimates it in 2000-2014. This indicates the difficulties when comparing short time periods with trends. ~~-~~Despite these uncertainties in the comparison to ARGO ~~data~~, it is clear that the models seem to have problems to realistically simulate the convection in the Labrador Sea. If deep convection occurs, the ocean is often mixed down to the bottom in the models, whereas~~ile in situ observations indicate that~~ deep convection rarely exceeds 2000m in the observations (Yashayaev and Loder, 2016; Yashayaev and Loder, 2017).

If we use a critical depth of z_{crit}=0 m instead of 1000 m in the Labrador Sea and thus consider the total mixed layer depth, the relative deviation of the DMV in the models from ARGO is reduced as expected (not shown). However, AWI-CM-1-0-LR and CMCC-CM2 still overestimate the DMV based on ARGO by a factor of three and two, respectively. On the other hand, ECMWF-IFS-LR simulates only 20% of the mixed volume compared to ARGO. The comparison between z_{crit0} and $z_{crit1000}$ reveals also some non-linearites in the deep convection. While CNRM-CM6.1-HR has a nine times higher DMV ($z_{crit1000}$) compared to ARGO, it is only 16% higher for z_{crit0}, whereas the DMV ($z_{crit1000}$) for MPI-ESM1-2-XR is 4.6 times higher compared to ARGO but 14% smaller for z_{crit0}.

The interannual variability of the DMV is large in all models (Figure 3). Some of the simulations (EC-Earth3P, HadGEM3-GC31-LL, MPI-ESM1-2, CNRM-CM6.1 and ECMWF-IFS-MR) also indicate substantial variability at decadal or longer periods~~. Despite missing continuous long-term observations of convection in the Labrador Sea, in situ observations from different observational campaigns suggest that deep convection occurs only intermittently with large interannual to decadal variations~~ where phases with and without convection alternate. Such intermittent deep convection was also suggested based

Formaterat: Teckensnitt:Inte Kursi
Formaterat: Teckensnitt:Inte Kursi

on observations (Lazier et al., 2002; Yashayaev and Loder, 2016)~~). Such intermittent deep convection is partly visible in the DMV time series of EC-Earth3P, HadGEM3-GC31-LL, MPI-ESM1-2, CNRM-CM6.1 and ECMWF-IFS-MR~~. However, in most of the model simulations, deep convection occurs in almost every winter or not at all.

The strength of the deep convection in March is reflected in the vertical density distribution in the Labrador Sea. To calculate the density, we used the definition of density following Millero and Poisson (1981). Naturally, the models with more frequent and deeper convection show a much weaker vertical stratification than the models that do not exhibit deep convection. We therefore analyse density profiles in the Labrador Sea in November that are not influenced by convection to explain why the mixed layer depth is overestimated in the following winter. ~~More interesting as the density distribution during the convection period itself is the vertical stratification at the beginning of the winter, which indicates the preconditioning of the ocean for convection events later in winter.~~ Figure 4 shows the vertical density stratification of the upper 600m in the Labrador Sea. All models show a near surface low density layer, mainly due to a combination of low surface salinity and relatively (compared to late winter) warm water near the surface in November. Generally, the models with lower ocean resolution show a stronger stratification in the upper ocean than models with higher resolution (except for AWI-CM-1-0). The two model simulations, which do not simulate any deep convection, ECMWF-IFS-LR and EC-Earth3P, show particularly strong upper ocean density gradients. Consequently, a large buoyancy flux would be needed during winter until deep convection could set in in these two models. MPI-ESM1-2 and AWI-CM-1-0 show a more stratified upper ocean in November with increased atmospheric resolution, which~~. This~~ agrees with a weaker convection in their higher resolution versions. The density profiles of the high ocean resolution models agree ~~relatively~~ well with the observed one from ARGO, although the near surface low density layer is too shallow in most of these models. This shallower surface layer requires less heat to be eroded, which might explain~~contribute to~~ the overestimation of the deep convection in late winter in these models (compare Figures 1 and 3). However, this~~but~~ is probably not the only reason as will be further discussed in section 4.

Twelve of 19 simulations indicate a significantly negative trend of the DMV in the historical period (Figure 3, Table 3). To investigate whether this trend is ~~really~~ due to external forcing or due~~and not to~~ to model drift~~ due to the rather short spinup period~~, we compared the DMV in the historical simulations with that from the 100-year 1950-control simulations (Figure 5 and Table 3). Most of the control simulations do not show any significant~~large~~ trend~~s~~ and in 9 out of 17 historical simulations, the DMV trends in the historical simulations are significantly more negative compared to the first 65 years of the control simulations. This ~~indicates~~ing that external forcing as~~is the~~ major cause for the DMV reduction in the historical simulations. Furthermore~~As found with the mean DMV~~, the negative trends become~~are~~ larger with higher ocean resolution~~ in the historic simulations.~~

A reduction of DMV in the historical period would be in line with some recent studies by Caesar et al. (2018), Thornalley et al. (2018) and Brodeau and Koenigk (2016).

To investigate the predominant variability frequency of the DMV, we calculated the power spectrum of detrended DMV time series of the Labrador Sea from the 100-year long control simulations ~~We calculated the power spectrum of the DMV in~~

Formaterat: Justera inte mellanrun mellan latinsk och asiatisk text, Juste inte mellanrum mellan asiatisk text o siffror

Formaterat: Teckensnitt:(Standard +Rubriker (Times New Roman)

Formaterat: Teckensnitt:(Standard +Rubriker (Times New Roman)

Formaterat: Teckensnitt:(Standard +Rubriker (Times New Roman)

Formaterat: Teckensnitt:(Standard +Rubriker (Times New Roman)

Formaterat: Teckensnitt:(Standard +Rubriker (Times New Roman)

~~the Labrador Sea in order to investigate the predominant variability of the DMV in each simulation in more detail~~ (Figure 6). ~~For better comparison, we detrended and normalized (using the standard deviation of the normalized time series) the 100-year 1950-control simulations.~~ The dominant time scale varies across simulations and models. Many of the models ~~with NEMO ORCA025 as the ocean model~~ (ECMWF-MR, HadGEM3-GC31-MM, HadGEM3-GC31-HM, ~~CMCC-CM2-HR~~, EC-Earth3P-HR~~,) and also~~ MPI-ESM1-2-HR) show a ~~dominant~~ peak in the spectrum at around 10 years. In ECMWFS-IFS-HR, HadGEM3-GC31-HH and MPI-ESM1-2-XR with further increased resolution in either ocean or atmosphere, the main peak in the spectrum seems to shift towards somewhat longer time periods. A shorter frequency of 7 years is found for CMCC-CM2-HR ~~The~~ and AWI-CM-1-0-HR ~~shows a very pronounced variation at a period of around 7 years~~. The lower ocean-resolution models, AWI-CM-1-0-LR, HadGEM3-GC31-LL and ECMWF-IFS-LR (but very weak DMV), show less dominate peaks than their higher resolution versions. CNRM-CM6.1 shows peaks at similar periods as CNRM-CM6.1-HR but the amplitudes differ.

3.2.2 ~~Greenland Sea~~GIN Seas

The DMV in the ~~Greenland Sea~~GIN Seas shows also a large spread across models (Figure 7, Table 2). As for the Labrador Sea, AWI-CM-1-0-LR and the two CMCC-CM2 simulations show the strongest deep convection while ECMWF-IFS and EC-Earth3P simulate rather weak convection (note the different order of magnitude in the vertical scales of Figure 7). ~~Only~~ MPI-ESM1-2-HR and CNRM-CM6.1 show the smallest deviations~~three out of seven models simulate Greenland Sea DMV's of a similar magnitude compared to~~ from the ARGO observations. ~~(~~HadGEM3-GC31-HM overestimates MLD by 70% when comparing the full historical period to ARGO (400% when comparing only 2000-2014) and~~,~~ MPI-ESM1-2-XR underestimates MLD by 50%~~, CNRM-CM6.1).~~ EC-Earth3P and ECMWF-IFS strongly underestimate deep water formation in the ~~Greenland Sea~~GIN Seas while the DMV is~~it is~~ strongly overestimated by AWI-CM-1-0 and CMCC-CM2.

The resolution dependency of ~~Greenland Sea~~ DMV in the GIN Seas differs substantially from the Labrador Sea. There is no robust relation between MLD and resolution. All models with NEMO show either no or shallower MLD with increased resolution. ~~The NEMO models do not show any deepening of convection with increased ocean resolution. In contrast, the high-resolution versions of ECMWF-IFS, EC-Earth3P and CNRM-CM6.1 (after 1980) show very shallow or no deep convection. Moving from HadGEM3-GC31-LL to HadGEM3-GC31-MM leads to substantially smaller DMV. However, when increasing the atmospheric resolution from HadGEM3-GC31-MM to HadGEM3-GC31-HM, DMV increases, and increases further in HadGEM3-GC31-HH, where both ocean and atmosphere resolution is increased. Thus, unlike for the Labrador Sea, there is no robust relation between the resolution in ocean or atmosphere and DMV in the Greenland Sea in the global models with NEMO as ocean component. The two other models,~~ MPI-ESM1-2 and AWI-CM-1-0 show, as for the Labrador Sea, a reduction of the DMV with increased resolution.

The trends of DMV in the ~~Greenland Sea~~GIN Seas ~~in the models~~ do not agree across models in the historical period (Figure 7, Table 3). While HadGEM3-GC31-MM, MPI-ESM1-2-XR and the CMCC-CM2 simulations show a significantly negative trend, HadGEM3-GC31-HM and EC-Earth3P show positive trends. This discrepancy could be due to the competing effects from~~that the~~ global warming~~. trend has on deep convection in the region~~, which are~~might be~~ represented differently in each model: on one hand, ~~by~~ reduce~~ding~~ sea ice extent ~~and thus~~ enable~~sing~~ a larger surface for deep convection, while~~, and~~ on the other hand ~~by releasing~~ melt~~ting heat~~ water ~~fluxes~~ and warme~~ring the ocean~~ surface water enhance the stratification~~, both contributing to lighter surface conditions and therefore increasing~~ and thus impede convection~~density stratification~~. The high DMV in CNRM-CM6.1-HR before 1970, and the decrease thereafter occurs similarly in the first decades of the 1950-control-simulation indicating that this trend is caused by a model balance adjustment and not due to external forcings (Figure 8, Table. 3). Similarly, the strong negative trends in CMCC-CM2 can partly be explained by similar drifts in the control simulations, although the reduction in the historical runs is significantly larger than in the control runs.

Some of the historical and control simulations show strong decadal or longer-term variations (Figure 9). HadGEM3-GC31-HM, MPI-ESM1-2-HR, AWI-CM-1-0-HR and EC-Earth3P-HR show dominant variability at periods of around 20-25 years; ECMWF-IFS-MR, HadGEM3-GC31-HH, CMCC-CM2 and CNRM-CM6-1 simulations at time scales of 10-15 years. In addition, some of the simulations indicate variability at time-scales below 8 years. Overall, there is no clear dependence of the variability on the resolution.

Figure 10 summarizes the results from sections 3.2.1 and 3.2.2. on the resolution dependency of the deep convection across the~~all seven~~ models in Labrador and GIN Seas. Each single model shows a clear dependence of the DMV in the Labrador Sea on the oceanic resolution. The differences across models are large, and as discussed before, even models using the same version of the NEMO as ocean model exhibit a wide range of solutions. Models with coarse resolution (~100 km) produce no or only shallow convection. Models with a resolution of 50km and higher in the ocean, however, overestimate deep convection compared to ARGO.~~Only models with coarse ocean resolution fail to produce any deep convection or produce only very shallow convection. All models with an ocean resolution of 50 km or higher (except for EC-Earth3P-HR) overestimate the convection compared to ARGO.~~

Increasing the atmosphere resolution has a minor impact on the DMV in the Labrador Sea, except for MPI-ESM1.2 and AWI-CM-1-0, where DMV is reduced with increased resolution.

The resolution dependency of the DMV in the ~~Greenland Sea~~GIN Seas in single models is smaller than in the Labrador Sea. However, all the models, except for CNRM-CM6-1, show a decreased DMV when increasing the resolution to around 0.25°. The response to increased atmosphere resolution is not robust across models.

4 The impact of heat and freshwater fluxes on the deep convection in the North Atlantic

Deep convection depends strongly on the buoyancy of the ocean surface layer in the convection regions - the heat loss to the atmosphere and the influx of fresh water into the convection regions.

4.1 Surface heat fluxes

Brodeau and Koenigk (2016) showed that the turbulent surface heat flux (SHF) is the main driver for interannual variability in the DMV. Thus, in the following, we will mainly focus on the SHF.

Figure 11 shows the winter (January, February, March) SHF in each of the model simulations. The WHOI-OAFlux data show the largest SHF (from the ocean to the atmosphere) up to more than 200 W/m^2 from the ice edge in the Labrador Sea extending to the southern part of the subpolar gyre, south of Iceland and along the southeast coast of Greenland, and in the northern Norwegian-Greenland Seas and Barents Sea. The large-scale features of this pattern are reproduced by most of the models. ECMWF-IFS-LR and to a lesser degree EC-Earth3P, both simulating too weak convection, strongly underestimate the SHF in the Labrador Sea. Increased ocean~~The high~~ resolution ~~models show a better~~improves the representation of the observed SHF pattern. In particularly, ~~they represent more realistically~~ the extension of high SHF from the Labrador Sea into the southwestern branch of the sub-polar gyre and the high SHF in the northern Greenland and Norwegian Seas is better simulated. A number of models (~~, in particular~~ both CMCC-CM2 versions, HadGEM3-GC31-HH and CNRM-CM6.1) overestimate the SHF in the sub-polar gyre. In addition, the SHF west and northwest of Scotland is too high in most of the models.

In the Labrador Sea, all high-resolution models with NEMO as the ocean component simulate increased SHF (averaged over the same box as used for calculation of the DMV) compared to their lower-resolution counterparts (Table 2). In contrast, MPI-ESM1-2 shows ~~a~~ reduced SHF with increased atmospheric resolution in line with the reduced convection. ~~This dependence shown by most models agrees well with the resolution dependency of the DMV in the Labrador Sea~~. In all models, the interannual variations of winter SHF ~~(averaged over the same box as used for calculation of the DMV)~~ is significantly positively correlated with the DMV in March. T~~h~~us, large ocean heat losses in the winter are linked to strong DMVs in the following March, indicating that large upward surface heat fluxes lead the DMV. The correlation coefficient varies from 0.48 in CNRM-CM6.1 to slightly above 0.7 in ECMWF-IFS-MR, EC-Earth3P and CMCC-CM2-HR4. The relation between SHF and DMV is neither resolution nor model dependent.

The winter SHF in the Labrador Sea itself is governed by the atmospheric circulation (not shown). In all model simulations northerly to northwesterly winds, which advect cold air from the Arctic sea ice towards the Labrador Sea, lead to strong surface heat fluxes, which overcome the stratification of the ocean (Ortega et al. 2011), and increased convection. These north-to-northwesterly winds are further linked to a large scale atmospheric circulation pattern, which is similar to the positive phase of the North Atlantic Oscillation (NAO, ~~),~~ defined as the leading EOF of geopotential height on the 500 hPa

Formaterat: Avstånd Före: 0 pt, efter: 0 pt

pressure surface over the European/Atlantic sector (80°W-40°E, 20°-90°N)). The spatial imprint of the NAO-index on the 500-hpa geopotential height is shown in Figure 12. All models reproduce the NAO-pattern of the ERA5-reanalysis data well. However, the position of the negative pole over Iceland-Greenland and the extension of the positive pole towards Eurasia vary slightly among models. The NAO-index itself, ~~which we define here as the difference of the normalized winter sea level pressure anomalies over the Azores and Iceland,~~ is significantly positively correlated with the DMV~~$_{z_{crit1000}}$~~ in the Labrador Sea in all simulations except for ~~the low resolution simulations with~~ EC-Earth3P and ECMWF-IFS. These are the simulations with no or only little deep convection and which have a strongly stratified ocean. The other model simulations show correlations between 0.38 (HadGEM-GC31-LL) and 0.67 (HadGEM-GC31-HM and CMCC-CM2-HR4). The NAO is not only important for interannual variations of the DMV but also on the decadal scale. Correlations of 10-year running means of NAO and DMV reach between 0.3 and 0.57. A spectral analysis of the NAO resembles most of the peaks in the spectrum of the DMV (not shown) although the NAO shows relatively more energy at shorter time scales compared to the DMV in the Labrador Sea.

~~As in the Labrador Sea, northerly winds are the main cause for large oceanic surface heat loss to the atmosphere in the Greenland Sea. The northerly winds are connected to low pressure anomalies over northern Scandinavia and the Barents Sea~~. As in the Labrador Sea, t~~T~~he DMV in the ~~Greenland Sea~~GIN Seas is correlated to the SHF as well and ocean heat loss is linked to a large DMV. Northerly winds are the main cause for large oceanic surface heat loss to the atmosphere in the GIN Seas. However, ~~here~~ we find a strong~~er~~er model dependency of the correlation than in the Labrador Sea~~is relation~~. The correlation is weak to moderate in HadGEM3-GC31 (r=0.22 for LL; r=0.5 for HH) and in CNRM-CM6.1 (r=0.35; r=0.5 for HH) but high correlation is found for ECWMF-IFS (r=0.64 for HR; r=0.85 in LR) and EC-Earth3P (r=0.61; r=0.69 for HR). As for the Labrador Sea, the relation between SHF and DMV shows no clear resolution -dependency.

4.2 Freshwater and sea ice exports

A number of studies have previously discussed the effect of Arctic freshwater export~~, especially through Fram Strait~~, as a potential source of variability of the deep water convection in the Labrador Sea (Holland et al., 2001; Jungclaus et al., 2005; Koenigk et al., 2006). Here, we analyze the correlations between freshwater transports across different sections (Fram Strait, Denmark Strait, northern Baffin Bay) and deep convection in the Labrador Sea as well as between~~nd~~ transports through Fram Strait and ~~deep convection in the Labrador Sea and in the Greenland Sea~~GIN Seas convection~~(transports through Fram Strait)~~ in the historical simulations of the models.

To calculate the liquid freshwater transport, we used the model grid lines on the native grids of the models that are closest to the geographical landmarks that define Fram Strait (across 78°N), Northern Baffin Bay (78°N) and Denmark Strait (66°N). The freshwater has been defined as the amount of zero-salinity water required to reach the observed salinity of a seawater sample starting from a reference salinity. Specifically, liquid freshwater transport (fwt, in m^3/s) is estimated as

Formaterat: Teckensnitt:Fet

Formaterat: Teckensnitt:(Standard +Rubriker (Times New Roman)

Formaterat: Teckensnitt:(Standard +Rubriker (Times New Roman)

Formaterat: Teckensnitt:(Standard +Rubriker (Times New Roman)

Formaterat: Radavstånd: 1,5 rade

Formaterat: Teckensnitt:(Standard +Rubriker (Times New Roman)

Formaterat: Teckensnitt:(Standard +Rubriker (Times New Roman)

Formaterat: Teckensnitt:(Standard +Rubriker (Times New Roman)

Formaterat: Teckensnitt:(Standard +Rubriker (Times New Roman)

Formaterat: Upphöjd

Formaterat: Teckensnitt:(Standard +Rubriker (Times New Roman)

$$fwt = \int_{p1}^{p2} \int_{D}^{\eta} \left(\frac{S - Sref}{Sref}\right) dzdx$$

for salinity S (in practical salinity units). As reference salinity Sref we used 34.80 psu for all models. The integration along z is performed from the bottom at depth D to the sea surface at height η (in this case η=0). p1 and p2 are the landmarks and the integration was done considering dx as the length (or depth for dz) between every grid point.

The~~We consider both the vertical integrated liquid freshwater transports and~~ solid freshwater transport is calculated from the ~~(~~sea ice~~)~~ transports across the sections assuming a constant ice salinity of 5 psu.

Table 4 shows the freshwater exports out of the Arctic into the North Atlantic through Fram Strait and Baffin Bay and through the Denmark Strait. Although differences between models are large, the exports through Fram Strait are generally larger than through Baffin Bay. The total freshwater exports through Fram Strait (liquid + solid export) varies between around 80000 m^3/s in the two CNRM-CM6.1 models and 160000 m^3/s in ECMWF-IFS-LR and HadGEM3-GC31-MM. The distribution between liquid and solid export through Fram Strait differs strongly across the simulations. While in HadGEM3-GC31-LL and all ECMWF-IFS and EC-Earth3P simulations most of the freshwater leaves the Arctic in the form of sea ice, liquid and solid parts are of similar size in the other models. In CNRM-CM6.1-HR, the liquid part is even larger than the solid part. The amount of freshwater that passes the Denmark Strait is reduced compared to Fram Strait in all models except for ECMWF-IFS-LR and MPI-ESM1.2-XR, and the liquid part is dominating. Large parts of the ice melt in the East Greenland Current on its way from Fram Strait to Denmark Strait.

The low resolution versions of ECMWF-IFS, HadGEM3-GC31, CNRM-CM6.1 show a larger fraction of solid exports through Fram Strait and larger liquid transports through Baffin Bay (EC-Earth3P as well for Baffin Bay) compared to their higher resolution counter parts. The sum of freshwater exports through Fram Strait and Baffin Bay differs more between the models than between different versions of single models. Despite the large differences in mean Arctic freshwater exports into the North Atlantic, there is no clear linkage to the mean DMV in GIN and Labrador Seas. Only for ECMWF-IFS-LR, we speculate that the very large freshwater fluxes, particularly in form of sea ice, through Denmark Strait contribute to the low surface density in the Labrador Sea (compare Figure 4) and consequently to suppress any deep convection activities in the Labrador Sea.

In order to further investigate if the variability of freshwater exports affects the deep convection in GIN and Labrador Seas, we correlate the~~Generally, the correlations between deep convection and both~~ solid and liquid transports across all sections with the DMV. ~~are relatively small although in some of the models significant.~~ In all model simulations, the annual mean southward transport of both liquid and solid freshwater across Fram Strait and the liquid transport across Denmark Strait are weakly negatively correlated with the deep convection in the Labrador Sea in March (~~. The correlation coefficients~~ ranginge

Formaterat: Teckensnitt:(Standard +Rubriker (Times New Roman)

Formaterat: Teckensnitt:(Standard +Rubriker (Times New Roman)

Formaterat: Teckensnitt:(Standard +Rubriker (Times New Roman)

Formaterat: Upphöjd

Formaterat: Upphöjd

between -0.1 and -0.4). The and reach highest correlation is reachedvalues when the freshwater transport through Fram Strait (and Denmark Strait) leads the convection by one to two years (zero to one year). Increased southward transport of sea ice and liquid freshwater transports through Fram Strait along Greenland's east coast and through Denmark Strait leads to more freshwater input into the Labrador Sea, which tends to reduce the convection. Figure 132 shows for the two model simulations with the highest correlation between freshwater transport through Denmark Strait and DMV in the Labrador Sea (HadGEM-GC31-LL, EC-Earth3P-HR) that increased freshwater transport reduce leads to a substantial reduction of the MLD in the Labrador region and thus contributes to the variability of the DMV. For most other model simulations, the effect of freshwater transports on the DMV is rather small. small compared to the impact of SHF variability on the DMV.

Formaterat: Teckensnitt:Inte Fet

In some models, the southward transport of liquid freshwater through Baffin Bay is positively correlated with the deep convection in the Labrador Sea (up to r=0.35 in HadGEM3-GC31-LL). This may seem counterintuitive, but northerly winds in the Baffin Bay cause strong SHF in the Labrador Sea and dominate the convective conditions and simultaneously lead to increased fresh water transports to the south.

We do not find any resolution dependency of the correlation between freshwater exports and convection in the Labrador Sea. This result is in contrast to a recent study from Fuentes Franco and Koenigk (2019) where they analyzed a set of HadGEM3-GC2 simulations at different resolutions and found larger correlations with increased resolution.

Overall, there is only a weak relationship between freshwater export through the Fram Strait and convection in the Greenland SeaGIN Seas, although it shows some dependency on the respective model (not shown). In some of the simulations, more freshwater export out of the Arctic is associated with reduced deep convection in the Greenland SeaGIN Seas, but in the majority of the simulations larger exports occur at the same time as increased convection. In the latter case, the increased convection is driven by northerly winds, which at the same time increase the freshwater exports through Fram Strait.

5 The linkage of the DMV to the AMOC

The effect of high resolution on the AMOC in the HighResMIP model simulations has been studied in more detail in a parallel study to ours (Roberts et al. acceptedsubmitted). They found that "the AMOC tends to become stronger as model resolution is enhanced, particularly when the ocean resolution is increased from non-eddying to eddy-present and eddy-rich". Roberts et al., (acceptedsubmitted) also analysed the relation between temporal mean values of the DMV and the average AMOC. As shown in our section 3.2, only few models simulate a DMV that is consistent to observed estimates. However, these models underestimate the AMOC (except for CNRM-CM6-1) compared to the RAPID-observations whereas some of the models (HadGEM3-GC31-MM and -HM, MPI-ESM1.2-HR, AWI-CM-1-0-LR) markedly overestimate the DMV in the Labrador Sea but simulate a realistic AMOC. Thus, the linkage between mean values of AMOC and DMV in the models is

not consistent with the observations. This indicates that other shortcomings in the representation of processes that govern the AMOC in the models exist. ~~Thus, the observations show a stronger AMOC with a lower DMV compared to the models, indicating other shortcomings in the representation of processes that govern the AMOC in the models.~~

There is in general a strong relationship between DMV in the Labrador Sea and the AMOC strength across models; models with more deep water production in the Labrador Sea have a stronger AMOC. Also for all single models (apart from AWI-CM-1-0), simulations with larger DMV are linked to a stronger AMOC. This relationship is less robust between DMV in the ~~Greenland Sea~~GIN Seas and the AMOC as expected from the reduced DMV with increased resolution in most of the models (see sections 3.2.2).

To investigate the impact of variability in the deep water formation on the variability of the AMOC, we performed cross-correlation analyses between the DMV in Labrador and ~~Greenland Sea~~GIN ~~s~~Seas and the AMOC (at 26°N) for lags between -/+ 10 years. In agreement with results by Brodeau and Koenigk (2016), annual values are only rather weakly correlated with each other. We thus focus here on correlations of linearly detrended and 10-year low pass filtered values of DMV and AMOC (Figures 1~~43~~ and 1~~54~~) in the 100-year 1950-control simulations. Positive lags mean that the AMOC leads DMV, negative lags mean that the DMV leads AMOC. In the case of Labrador Sea (Figure 1~~43~~), maximum values of the normalized cross-correlations vary between around 0.3 (AWI-CM-1-0-HR, ECMWF-IFS-MR, CMCC-CM2-HR, EC-Earth3P-HR) and 0.8 (HadGEM3-GC31-LL, CMCC-CM6-1-VHR). Also CNRM-CM61-HR and MPI-ESM1-2-XR and HadGEM3-GC31-HM (HH) show high correlations. Most model simulations with high correlations reach their maximum correlation when the DMV leads the AMOC by 0-4 years.

The cross-correlations between DMV in the ~~Greenland Sea~~GIN Seas and the AMOC index are generally positive for lags around year 0 but somewhat lower compared to the Labrador Sea. Relatively high values (exceeding 0.6) are obtained for the HadGEM3-GC31 model versions and by CNRM-CM6-1-HR. The time lag where correlations are highest differ among models. While in AWI-CM-1.0-models, CMCC-CM2-VHR and MPI-ESM1.2-HR, the DMV in the ~~Greenland Sea~~GIN Seas leads the AMOC by a few years, in HadGEM-GC31 simulations and EC-Earth3P-HR, the AMOC leads the DMV, and in the other simulations no clear lead-lag relation can be identified.

6 Conclusions

We analyzed historical and 1950-control simulations in different resolution from seven global climate models following the HighResMIP protocol and investigated the impact of increasing the resolutions in ocean and atmosphere on deep convection in the North Atlantic Ocean.

The main results are summarized as follows:

- In general, global models mostly fail to simulate a realistic deep convection in the North Atlantic. This is critical since a realistic simulation of deep convection is important for the large scale ocean circulation, in particular the AMOC, the northward heat transport in the ocean and related impacts on the atmosphere. It also raises serious questions of the future behaviour of the AMOC in climate models and its consequences for local and global climate.

- The ocean resolution clearly affects the deep water formation in the Labrador Sea. Convection activity enhances with increasing ocean resolution in four out of five models in this study. However, all these models use NEMO3.6 (although in somewhat different configurations) as their ocean component. It remains therefore unclear whether global models with other ocean models respond differently to an increased resolution since the reduced convection in the fifth model (AWI-CM-1-0) results very likely from the simultaneously increased atmosphere resolution.

- Increasing the ocean resolution from 1° to 1/4° in the models with NEMO as the ocean component has a larger impact on the convection than increasing the atmosphere resolution in these models. In contrast, MPI-ESM1-2, in which only the atmosphere resolution has been increased, and AWI-CM-1-0 (increased resolution in both atmosphere and ocean) show substantially reduced convection in the Labrador Sea at high resolution. Both models (AWI-CM-1-0, MPI-ESM1-2) use the same atmospheric component (ECHAM6.3) and the reduction of DMV with increased atmospheric resolution can likely be linked to reduced atmospheric winds in ECHAM6.3 in the high resolution version (Gutjahr et al., 2019; Putrasahan et al., 2019). The models with higher ocean resolution show more dominate variability at the decadal time scale in the Labrador Sea compared to their lower resolution counterparts.

- In the ~~Greenland Sea~~GIN Seas, increasing the ocean model resolution to around 1/4° reduces the convection in most models. Increasing the atmosphere resolution tends to reduce the convection but the result is not robust across models. Many models show dominant variability between 10 and 25 years but no clear dependence on the resolution could be found.

- The turbulent surface heat fluxes are strongly related to the deep convection in both the Labrador and ~~Greenland Sea~~GIN ~~s~~Seas and seem to be more important for the variability of the DMV than freshwater exports out of the Arctic. In the Labrador Sea, we find that higher resolution leads to increased ocean heat release to the atmosphere in all the NEMO models but to reduced heat release in MPI-ESM1-2. This is in close agreement with the resolution dependency of the deep convection. Thus, increased turbulent surface heat flux with high resolution is the main explanation for increased DMV in the Labrador Sea. The correlation between surface heat fluxes and DMV in the Labrador and ~~Greenland Sea~~GIN ~~s~~Seas does not show any robust resolution-dependency.

- The 10-year low pass filtered DMV in the Labrador Sea is highly positively correlated (r=0.6-0.8) with the AMOC at 26 °N in around half of the model simulations. In these simulations, the DMV leads the AMOC by a few years. In the other

simulations, the correlations are also positive but much lower (0.3-0.4) and time lags of the highest correlations are not robust across these simulations. The DMV in the ~~Greenland Sea~~GIN Seas and the AMOC are only significantly correlated in few simulations and no clear lead/ lag relationship can be established. The correlations between DMV and AMOC are not dependent on the resolution.

- Increasing the resolution improves the vertical stratification of the upper ocean in late autumn but it does not generally improve the representation of the deep convection. In a few of the low-resolution models, the convection is overestimated compared to ARGO and this positive bias becomes even larger with higher resolution. However, the high resolution models have not been tuned and the main purpose of HighResMIP is to investigate the impact of increasing the resolution rather than to improve existing biases.

Acknowledgements

This work has been funded by PRIMAVERA project, which is funded by the European Union's Horizon 2020 programme, Grant Agreement no. 641727PRIMAVERA.

The global ocean heat flux and evaporation products were provided by the WHOI OAFlux project (http://oaflux.whoi.edu) funded by the NOAA Climate Observations and Monitoring (COM) program.

Data: The data are stored on the Jasmin infrastructure, http://www.ceda.ac.uk/projects/jasmin/. The simulations are part of the High Resolution Model Intercomparison project (HiResMIP) and will be uploaded to the ESGF: https://esgf-node.llnl.gov

Scripts for analyzing the data will be available from the corresponding authors upon reasonable request.

Authors' contributions: TK is first author of the manuscript and performed the largest part of the analysis, RFF calculated the freshwater exports out of the Arctic, VLM calculated the AMOC and contributed with the analysis between DMV and AMOC. OG, LJ, AN, PO, CR, MR, TA, DI, MM and DS contributed with discussions on the processes governing the DMV and linking DMV and AMOC as well as with performing the model simulations.

References

Ba, J., Keenlyside, N.S., Latif, M., Park, W., Ding, H., Lohmann, K., Mignot, J.,Menary, M., Ottera, O.H., Wouters, B., Salas y Melia, D., Oka, A., Bellucci, A., Volodin, E.: A multi-model comparison of Atlantic multidecadal variability, Clim. Dyn., 43, 2333–2348, DOI:10.1007/s00382-014-2056-1, 2014.

Biastoch, A., Böning, C.W., Getzlaff. J, Molines, J.M., and Madec, G.: Causes of interannual-decadal variability in the meridional overturning circulation of the midlatitude North Atlantic ocean, J. Clim., 21:6599–6615, doi:10.1175/2008JCLI2404.1, 2008.

Brodeau, L., and Koenigk, T.: Extinction of the northern oceanic deep convection in an ensemble of climate model simulations of the 20th and 21st centuries, Clim. Dyn. 46, 2863, doi:10.1007/s00382-015-2736-5, 2016.

Caesar, L., Rahmstorf, S., Robinson, A., Feulner, G., and Saba, V.: Observed fingerprint of a weakening Atlantic Ocean overturning circulation, Nature, 556, 191-196, https://doi.org/10.1038/s41586-018-0006-5, 2018.

Chassignet, E.P., and D.P. Marshall 2008: Gulf Stream Separation in Numerical Ocean Models. Ocean Modeling in an Eddying Regime, Geophysical Monograph Series 177, doi: 10.1029/177GM05.

Cheng, W, Chiang, J.C.H., and Zhang, D.: Atlantic Meridional Overturning Circulation (AMOC) in CMIP5 Models: RCP and Historical Simulations, J. Clim., 26, 7187-7197, DOI: 10.1175/JCLI-D-12-00496.1, 2013.

Cherchi, A., Fogli, P. G., Lovato, T., Peano, D., Iovino, D., Gualdi, S., Masina, S., Scoccimarro, E., Materia, S., Bellucci, A., and Navarra, A.: Global mean climate and main patterns of variability in the CMCC-CM2 coupled model, J. Adv. Model. Earth Sy., 11, 185–209, https://doi.org/10.1029/2018MS001369, 2019.

Clarke, R., and Gascard, J.: The formation of Labrador Sea Water. Part 1: Large-scale processes. Journal of Physical Oceanography 13, 1764–1778, 1983.

de Boyer Montégut, C., Madec, G., Fischer, A. S., Lazar, A., and Iudicone, D.: Mixed layer depth over the global ocean: An examination of profile data and a profile-based climatology, J. Geophys. Res., 109, C12003, doi:10.1029/2004JC002378, 2004.

de Jong, M. F., and de Steur, L.: Strong winter cooling over the Irminger Sea in winter 2014–2015, exceptional deep convection, and the emergence of anomalously low SST, Geophys. Res. Lett., 43, 7106–7113, doi:10.1002/ 2016GL069596, 2016.

de Jong, M. F., Oltmanns, M., Karstensen, J., and de Steur, L.: Deep convection in the Irminger Sea observed with a dense mooring array. Oceanography, 31(1), 50-59, doi: 10.5670/oceanog.2018.109, 2018.

Deser, C., Holland, M., Reverdin, G., and Timlin, M: Decadal variations in Labrador Sea ice cover and North Atlantic sea surface temperatures, J Geophys. Res. 107 (C5), 3035, doi:10.1029/2000JC000683, 2002.

Deshayes, J., Frankignoul, C., and Drange, H.: Formation and export of deep water in the Labrador and Irminger seas in a GCM, Deep Sea Res., 54, 510–532, 2007.

Formaterat: Nivå 1, Avstånd Före: 24 pt, efter: 12 pt, Radavstånd: enkelt, Håll ihop med nästa

Formaterat: Teckenfärg: Svart, Kerning från 16 pt

Dickson, R.R., and Brown, J.: The production of North Atlantic Deep Water: sources, rates, and pathways, J. Geophys. Res., 99(C6), 12319–12341, doi:10.1029/94jc00530, 1994.

Docquier, D., Grist, J.P., Roberts, M.J., Roberts, C. D., Semmler, T., Ponsoni, L., Massonnet, F., Sidorenko, D., Sein, D.V., Iovino, D., Bellucci, A., and Fichefet, T.: Impact of model resolution on Arctic sea ice and North Atlantic Ocean heat transport, Clim. Dyn. 53, 4989–5017, https://doi.org/10.1007/s00382-019-04840-y, 2019.

Docquier, D., Fuentes-Franco, R., Koenigk, T., and Fichefet, T.: Sea ice - ocean interactions in the Barents Sea modeled at different resolutions, Front. Earth Sci. 8:172, doi: 10.3389/feart.2020.00172.

Eden, C., and Willebrand, J.: Mechanism of interannual to decadal variability of the North Atlantic circulation, J. Clim., 14(10), 2266–2280, doi:10.1175/1520-0442(2001)014, 2001.

Fox-Kemper, B., Adcroft, A., Böning, C. W., Chassignet, E. P., Curchitser, E., Danabasoglu, G. Eden, C. and co-authors: Challenges and Prospects in Ocean Circulation Models, Front. Mar. Sci., 26, https://doi.org/10.3389/fmars.2019.00065, 2019.

Frankignoul, C., Deshayes, J., and Curry, R.: The role of salinity in the decadal variability of the North Atlantic meridional overturning circulation, Clim. Dyn., 33, 777–793, doi:10.1007/s00382-008-0523-2, 2009.

Franco Fuentes, R., Koenigk, T.: Sensitivity of the Arctic fresh water budget to model resolution, Clim. Dyn., published online, doi: 10.1007/s00382-019-04735-y, 2019.

Gelderloos, R., Straneo, F., and Katsman, C.A.: Mechanisms behind the temporary shutdown of deep convection in the Labrador sea: lessons from the great salinity anomaly years 1968–71, J. Clim., 25,6743–6755, doi:10.1175/JCLI-D-11-00549.1, 2012.

Gutjahr, O., Putrasahan, D., Lohmann, K., Jungclaus, J. H., von Storch, J.-S., Brüggemann, N., Haak, H., and Stössel, A.: Max Planck Institute Earth System Model (MPI-ESM1.2) for the High-Resolution Model Intercomparison Project (HighResMIP), Geosci. Model Dev., 12, 3241–3281, https://doi.org/10.5194/gmd-12-3241-2019, 2019.

Haarsma, R. J., Roberts, M. J., Vidale, P. L., Senior, C. A., Bellucci, A., Bao, Q., Chang, P., Corti, S., Fučkar, N. S., Guemas, V., von Hardenberg, J., Hazeleger, W., Kodama, C., Koenigk, T., Leung, L. R., Lu, J., Luo, J.-J., Mao, J., Mizielinski, M. S., Mizuta, R., Nobre, P., Satoh, M., Scoccimarro, E., Semmler, T., Small, J., and von Storch, J.-S.: High Resolution Model Intercomparison Project (HighResMIP v1.0) for CMIP6, Geosci. Model Dev., 9, 4185–4208, https://doi.org/10.5194/gmd-9-4185-2016, 2016.

Haarsma, R., Acosta, M., Bakhshi, R., Bretonnière, P.-A. B., Caron, L.-P., Castrillo, M., Corti, S., Davini, P., Exarchou, E., Fabiano, F., Fladrich, U., Fuentes Franco, R., García-Serrano, J., von Hardenberg, J., Koenigk, T., Levine, X., Meccia, V., van Noije, T., van den Oord, G., Palmeiro, F. M., Rodrigo, M., Ruprich-Robert, Y., Le Sager, P., Tourigny, É., Wang, S., van Weele, M., and Wyser, K.: HighResMIP versions of EC-Earth: EC-Earth3P and EC-Earth3P-HR. Description, model performance, data handling and validation, Geosci. Model Dev. Discuss., https://doi.org/10.5194/gmd-2019-350, in review, 2020.

Formaterat: Teckensnitt:Inte Fet

Formaterat: Teckensnitt:Inte Fet

Formaterat

Heuzée, C.: North Atlantic deep water formation and AMOC in CMIP5 models. Ocean Sci., 13, 609–622, https://doi.org/10.5194/os-13-609-2017, 2017.

Heuzé, C.: Antarctic Bottom Water and North Atlantic Deep Water in CMIP6 models, Ocean Sci. Discuss., https://doi.org/10.5194/os-2020-66, in review, 2020.

Holland, M.M., Bitz, C.M,. Eby, M., and Weaver, A.J.: The role of ice-ocean interactions in the variability of the North Atlantic thermohaline circulation, J. Clim., 14, 656–675, doi:10.1175/1520-0442(2001)014, 2001.

Holte, J., Talley, L. D., Gilson, J., and Roemmich, D.: An Argo mixed layer climatology and database, Geophys. Res. Lett., 44, 5618–5626, https://doi.org/10.1002/2017GL073426, 2017.

Jackson, L.C., Kahana, R., Graham, T., Ringer, M.A., Woollings, T., Mecking, J.V., and Wood, R. A.: Global and European climate impacts of a slowdown of the AMOC in a high resolution GCM, Clim. Dyn., 45, 3299–3316, DOI:10.1007/s00382-015-2540-2, 2015.

Jackson, L.C., Peterson, K., Roberts, C., and Wood, R. A.: Recent slowing of Atlantic overturning circulation as a recovery from earlier strengthening, Nature Geosci. 9, 518–522, https://doi.org/10.1038/ngeo2715, 2016.

Jungclaus, J., Haak, H., Latif, M., and Mikolajewicz, U.: Arctic-North Atlantic interactions and multidecadal variability of the meridional overturning circulation, J. Clim., 18,4013–4031, doi:10.1175/JCLI3462.1, 2005.

Koenigk ,T., Mikolajewicz, U., Haak, H., and Jungclaus, J.: Variability of Fram Strait sea ice export: causes, impacts and feedbacks in a coupled climate model, Clim. Dyn., 26,17–34, doi:10.1007/s00382-005-0060-1, 2006.

Koenigk, T., Mikolajewicz, U., Haak, H., and Jungclaus, J.: Arctic freshwater export in the 20th and 21st centuries, J. Geophys. Res., doi:10.1029/2006JG000274, 2007.

Koenigk, T., C. König Beatty, M Caian, R. Döscher, and Wyser, K.: Potential decadal predictability and its sensitivity to sea ice albedo parameterization in a global coupled model, Clim. Dyn., 38(11-12), 2389-2408, DOI: 10.1007/s00382-011-1132-z, 2012.

Koenigk, T., and Brodeau, L.: Arctic climate and its interaction with lower latitudes under different levels of anthropogenic warming in a global coupled climate model, Clim. Dyn., 49(1-2): 471-492, doi:10.1007/s00382-016-3354-6, 2017.

Kuhlbrodt, T., Griesel, A., Montoya, M., Levermann , A., Hofmann, M., and Rahmstorf, S.: On the driving processes of the Atlantic meridional overturning circulation, Rev. Geophys., doi:10.1029/2004RG0001662007, 2007.

Langehaug, H.R., Medhaug, I., Eldevik, T., Otterå, O.H.: Arctic/ Atlantic exchanges via the Subpolar Gyre, J. Clim., 25(7), 2421–2439, doi:10.1175/jcli-d-11-00085.1, 2012.

Latif, M., Böning, C., Willebrand, J., Biastoch, A., Dengg, J., Keenlyside, N.,Schweckendiek, U.,and Madec, G.: Is the thermohaline circulation changing? J. Clim., 19,4631–4637, doi:10.1175/JCLI3876.1, 2006.

Lavergne, C., Palter, J.B., Galbraith, E.D., and Bernardello, R., and Marinov, I.: Cessation of deep convection in the open southern ocean under anthropogenic climate change, Nat. Clim. Change, 4, 278–282. doi:10.1038/nclimate2132, 2014.

Levitus, S.: Climatological atlas of the world ocean, U.S. Government Printing Office 13, NOAA, Washington, D.C., 163 pp., 1982.

L'Hévéder, B., Li, L., Sevault, F., and Somot, S.: Interannual variability of deep convection in the Northwestern Mediterranean simulated with a coupled AORCM, Clim. Dyn., 41(3-4), 937–960, doi:10.1007/s00382-012-1527-5, 2012.

Lozier, M.S., S. Bacon, A.S. Bower, S.A. Cunningham, M. F. de Jong, L. de Steur, B. deYoung, J. Fischer, S.F. Blair, J.W. Greenan, P. Heimbach, N.P. Holiday, L. Houpert, M.E. Inall, W.E. Johns, H.L. Johnson, J. Karstensen, F. Li, X. Lin, N. McKay, D.P. Marshall, H. Mercier, P.G. Myers, R.S. Pickart, H.R. Pillar, F. Straneo, V. Thierry, R.A. Weller, R.G. Williams, C. Wilson, J. Yang, J. Zhao, D. Zika 2017. Overturning in the subpolar North Atlantic Program: A new international Ocean Observing System. BAMS, 737-752, https://doi.org/10.1175/BAMS-D-16-0057.1, 2017.

Lozier M.S., Li F., Bacon, S., Bahr, F., Bower, A. S., Cunningham, S. A., de Jong, M. F., de Steur, L., deYoung, B., Fischer, J., Gary, S.F., Greenan, B. J. W., Holliday, N. P., Houk, A., Houpert, L., Inall, M. E., Johns, W. E., Johnson, H. L., Johnson, C., Karstensen, J., Koman, G., Le Bras, I. A., Lin, X., Mackay, N., Marshall, D. P., Mercier, H., Oltmanns, M., Pickart, R. S., Ramsey, A. L., Rayner, D., Straneo, F., Thierry, T., Torres, D. J., Williams, R. G., Wilson, C., Yang, J., Yashayaev, I., and Zhao, J: A sea change in our view of overturning in the subpolar North Atlantic, Science 363, 516–521, 2019.

Mahajan, S., Zhang R., and Delworth, T.: Impact of the Atlantic Meridional Overturning Circulation (AMOC) on Arctic Surface Air Temperature and Sea Ice Variability, J. Clim., 24, 6573-6581, DOI: 10.1175/2011JCLI4002.1, 2011.

Manabe, S., and Stouffer, R.J.: The role of thermohaline circulation in climate, Tellus B,51, 91-109, https://doi.org/10.1034/j.1600-0889.1999.00008.x, 1999.

Marotzke, J., Scott, J.R.: Convective mixing and the thermohaline circulation. J. Phys. Oceanogr. 29(11), 2962–2970, doi:10.1175/1520-0485(1999)029, 1999.

Marshall, J., Schott, F.: Open-ocean convection: observations, theory, and models, Rev. Geophys., 37,1–64, doi:10.1029/98RG02739, 1999.

Medhaug, I., and Furevik, T.: North Atlantic 20th century multidecadal variability in coupled climate models: sea surface temperature and ocean overturning circulation, Ocean Sci., 7, 389–404, doi:10.5194/os-7-389-2011, 2011.

Millero, F. J., and Poisson, A.: International one-atmosphere equation of state of seawater. Deep Sea Research Part A. Oceanographic Research Papers 28 (6), 625-629, https://doi.org/10.1016/0198-0149(81)90122-9, 1981.

Ortega, P., Hawkins, E., and Sutton, R. Processes governing the predictability of the Atlantic meridional overturning circulation in a coupled GCM, Clim. Dyn. 37, 1771–1782, https://doi.org/10.1007/s00382-011-1025-1, 2011.

Putrasahan, D. A., Lohmann, K., von Storch, J.-S., Jungclaus, J. H., Gutjahr, O., and Haak, H.: Surface flux drivers for the slowdown of the Atlantic Meridional Overturning Circulation in a high-resolution global coupled climate model. Journal of Advances in Modeling Earth Systems, 11, 1349–1363. https://doi.org/10.1029/ 2018MS001447, 2019.

Roberts, C. D., Garry, F. K., and Jackson, L. C.: A Multimodel Study of Sea Surface Temperature and Subsurface Density Fingerprints of the Atlantic Meridional Overturning Circulation, J. Clim. 26, 9154-9174, https://doi.org/10.1175/JCLI-D-12-00762.1, 2013.

Roberts, C. D., Jackson, L., an McNeall, D.: Is the 2004–2012 reduction of the Atlantic meridional overturning circulation significant? Geophys. Res. Lett.,41, 3204–3210, doi:10.1002/2014GL059473, 2014.

Roberts, C.D., Senan R. , Molteni F. , Boussetta S., Mayer M. , and Keeley, S. P. E.: Climate model configurations of the ECMWF Integrated Forecasting System (ECMWF-IFS cycle 43r1) for HighResMIP, Geosci. Model Dev., 11, 3681–3712, https://doi.org/10.5194/gmd-11-3681-2018, 2018.

Roberts, M. J., Baker, A., Blockley, E. W., Calvert, D., Coward, A., Hewitt, H. T., Jackson, L. C., Kuhlbrodt, T., Mathiot, P., Roberts, C. D., Schiemann, R., Seddon, J., Vannière, B., and Vidale, P. L.: Description of the resolution hierarchy of the global coupled HadGEM3-GC3.1 model as used in CMIP6 HighResMIP experiments, Geosci. Model Dev., https://doi.org/10.5194/gmd-12-4999-2019, 2019.

Roberts, M.J., L. C. Jackson, C. D. Roberts, V. Meccia, D. Docquier, T. Koenigk, P. Ortega, E. Moreno-Chamarro, A. Bellucci, A. Coward, S. Drijfhout, E. Exarchou, O. Gutjahr, H. Hewitt, D. Iovino, K. Lohmann, R. Schiemann, J. Seddon, L. Terray, X. Xu, Q. Zhang, P. Chang, S. G. Yeager, F. S. Castruccio, S. Zhang, L. Wu, accepted: Sensitivity of the Atlantic Meridional Overturning Circulation to Model Resolution in CMIP6 HighResMIP Simulations and Implications for Future Changes. Journal of Advances in Modeling Earth Systems

Robson, J., Ortega, P., and Sutton, R.: A reversal of climatic trends in the North Atlantic since 2005, Nature Geosci. 9, 513–517, https://doi.org/10.1038/ngeo2727, 2016.

Rudels, B., and Quadfasel, D.: The Arctic Ocean Component in the Greenland-Scotland overflow. Journal of Marine Systems 2 (3–4), 435-450, https://doi.org/10.1016/0924-7963(91)90045-V, 1991.

Ronski, S., and Budéus, G.: Time series of winter convection in the Greenland Sea, J. Geophys. Res., 110, C04015, doi:10.1029/2004JC002318, 2005.

Sayol, J.M., Dijkstra, H. , and Katsman, C.: Seasonal and regional variations of sinking in the subpolar North Atlantic from a high-resolution ocean model. Ocean Sci., 15, 1033–1053, https://doi.org/10.5194/os-15-1033-2019, 2019.

Schott, F.A., Stramma, L., Giese, B.S., and Zantopp, R.: Labrador Sea convection and subpolar North Atlantic deep water export in the SODA assimilation model, Deep Sea Res., 56, 926–938, doi:10.1016/j.dsr.2009.01.001, 2009.

Sein, D.V., Danilov, S., Biastoch, A., Durgadoo, J.V., Sidorenko, D., Harig, S. and Wang, Q.: Designing variable ocean model resolution based on the observed ocean variability, Journal of Advances in Modeling Earth Systems, 8 (2), 904-916, doi:10.1002/2016MS000650, 2016.

Sein, D. V. , Koldunov, N. V., Danilov, S., Sidorenko, D., Wekerle, C., Cabos, W., Rackow, T., Scholz, P., Semmler, T., Wang, Q. and Jung, T.: The Relative Influence of Atmospheric and Oceanic Model Resolution on the Circulation of the North Atlantic Ocean in a Coupled Climate Model. Journal of Advances in Modeling Earth Systems, Doi:10.1029/2018MS001327, 2018.

Sidorenko, D., Rackow, T., Jung, T., Semmler, T., Barbi, D., Danilov, S., Dethloff, K., Dorn, W., Fieg, K., Gößling, H. F., Handorf, D., Harig, S., Hiller, W., Juricke, S., Losch, M., Schröter, J., Sein, D.V. and Wang, Q.: Towards multi-resolution global climate modeling with ECHAM6–FESOM. Part I: model formulation and mean climate, Climate Dynamics, doi: 10.1007/s00382-014-2290-6, 2014.

Formaterat: Teckensnitt:10 pt, Int
Fet

Formaterat: Avstånd efter: 8 pt, Radavstånd: 1,5 rader

Formaterat: Teckensnitt:10 pt

Formaterat: Teckensnitt:10 pt

Smeed, D. A., McCarthy, G. D., Cunningham, S. A., Frajka-Williams, E., Rayner, D., Johns, W. E., Meinen, C. S., Baringer, M. O., Moat, B. I., Duchez, A., and Bryden, H. L.: Observed decline of the Atlantic meridional overturning circulation 2004–2012, Ocean Sci., 10, 29–38, https://doi.org/10.5194/os-10-29-2014, 2014.

Smeed, D. A., Josey, S. A., Beaulieu, C.,Johns, W. E., Moat, B. I., Frajka-Williams, E., Rayner, D., Meinen, C. S., Baringer, M. O., Bryden, H. L. and McCarthy, G. D.: The North Atlantic Oceanis in a state of reduced overturning, Geophys. Res. Lett., 45, 1527–1533, https://doi.org/10.1002/2017GL07635, 2018.

Swingedouw, D., Braconnot, P., Delecluse, P., Guilyardi, E., and Marti, O.: Quantifying the AMOC feedbacks during a $2xCO_2$ stabilization experiment with land-ice melting, Clim. Dyn., 29, 521–534, DOI 10.1007/s00382-007-0250-0, 2007.

Thornalley, D., J. R., Oppo, D.,W. , Ortega, P., Robson, J. I., Brierley, C.,M., Davis, R., Hall. I. R.,Moffa-Sanchez, P., Rose, N.L., Spooner, P.T., Yashayaev. I., and Keigwin, L.D.: Anomalously weak Labrador Sea convection and Atlantic overturning during the past 150 years, Nature, 556, 227-231, https://doi.org/10.1038/s41586-018-0007-4, 2018.

Torrence, C., and Compo, G. P.: A Practical Guide to Wavelet Analysis, Bulletin of the American Meteorological Society 79 (1), 61-78, 1998.

Vannière, B., Demory, M. E., Vidale, P. L., Schiemann, R., Roberts, M. J., Roberts, C. D., Matsueda, M., Terray, L., Koenigk, T., and Senan, R.: Multi-model evaluation of the sensitivity of the global energy budget and hydrological cycle to resolution. Clim. Dyn., 52(11), 6817-6846, doi:10.1007/s00382-018-4547-y , 2019.

Voldoire, A., Saint-Martin, D., Sénési, S., Decharme, B., Alias, A., Chevallier, M., Colin, J., Guérémy, J.-F., Michou, M., Moine, M.-P., Nabat, P., Roehrig, R., Salas y Mélia, D., Séférian, R., Valcke, S., Beau, I., Belamari, S., Berthet, S., Cassou, C., Cattiaux, J., Deshayes, J., Douville, H., Franchisteguy, L., Ethé, C., Geoffroy, O., Lévy, C., Madec, G., Meurdesoif, Y., Msadek, R., Ribes, A., Sanchez-Gomez, E., and Terray,L.: Evaluation of CMIP6 DECK Experiments with CNRM-CM6-1. J. Adv. Model. Earth Syst., 11, 2177–2213, https://doi.org/10.1029/2019MS001683, 2019.

Yashayaev, I.: Hydrographic changes in the Labrador Sea, 1960-2005, Prog. Oceanogr. 73(3-4), 242-276, doi:10.1016/j.pocean.2007.04.015, 2007.

Yashayaev, I., and Loder, J.W.: Enhanced production of Labrador Sea Water in 2008, Geophys. Res. Lett., doi:10.1029/2008gl036162, 2009.

Yashayaev, I., and Loder, J. W.: Recurrent replenishment of Labrador Sea Water and associated decadalscale variability, J. Geophys. Res. Oceans, 121, 8095–8114, doi:10.1002/ 2016JC012046, 2016.

Yashayaev, I., and Loder, J. W.: Further intensification of deep convection in the Labrador Sea in 2016, Geophys. Res. Lett., 44, 1429–1438, doi:10.1002/2016GL071668, 2017.

Model	Ocean Model resolution	Atmosphere Model resolution	hist runs 1950-2014	100-yr ctrl-1950
	NEMO3.4/ LIM2	IFS cycle 43r1		
ECMWF-IFS-LR	ORCA1 - 1°	50 km	6	1
ECMWF-IFS-MR	ORCA025 – 1/4°	50 km	1	1
ECMWF-IFS-HR	ORCA025 – 1/4°	25 km	4	1
	NEMO3.6/ CICE5.1	UM		
HadGEM3-GC31-LL	ORCA1 - 1°	130 km	1	1
HadGEM3-GC31-MM	ORCA025 – 1/4°	60 km	1	1
HadGEM3-GC31-HM	ORCA025 - 1/4°	25 km	1	1
HadGEM3-GC31-HH	ORCA12 - 1/12°	25 km	1	1
	MPIOM1.6.3	ECHAM6.3		
MPI-ESM1-2-HR	TP04 - 0.4°	T127	1	1
MPI-ESM1-2-XR	TP04 – 0.4°	T255	1	1

	NEMO3.6/CIC4.0	CAM4		
CMCC-CM2-HR4	ORCA025 -1/4°	100 km	1	1
CMCC-CM2-VHR4	ORCA025 - 1/4°	25 km	1	1
	NEMO3.6/GELATO	ARPEGE6.3		
CNRM-CM6-1	ORCA1 - 1°	T127	1	1
CNRM-CM6-1-HR	ORCA025 - 1/4°	T359	1	1
	FESOM	ECHAM6.3		
AWI-CM-1-0-LR	50 km	T63	1 (-2010)	1
AWI-CM-1-0-HR	25 km	T127	1 (-2010)	1
	NEMO3.6/LIM3	IFS cycle 36r4		
EC-Earth3P	ORCA1 - 1°	T255	1	1
EC-Earth3P-HR	ORCA025 - 1/4°	T511	1	1

Table 1: Overview on the model configurations and the simulations used in this study.

~~**Normalized DMV, SHF**~~	**DMV$_{ratio\,norm}$ Lab-Sea**	**SHF$_{ratio\,norm}$ Lab-Sea**	**DMV$_{ratio\,norm}$ GIN~~reen~~-Sea**	**SHF$_{ratio\,norm}$ GIN~~reen~~-Sea**	**Corr SHF-DMV Lab-Sea**	**Corr SHF-DMV GIN~~reen~~-Sea**
ARGO/ WHOI Observations absolute values	3.95e+13 m^3	129.2 W/m^2	6.5e+13 m^3	125.7 W/m^2	not enough data	not enough data
ECMWF-IFS-LR	0.02 ~~0.03~~ (0.03)	0.53~~40 0.65~~	0~~.0.008~~ (0)	0.56~~45 0.68~~	0.62	0.85
ECMWF-IFS-MR	8.9 (4.9)	1.15	0~~.0002~~ (0)	0.93	0.71	0.65
ECMWF-IFS-HR	10.7~~9.9 11.7~~ (9.9)	1.21~~17 1.26~~	0~~.0.002~~ (0)	0.85~~3 0.87~~	0.59	0.64
HadGEM3-GC31-LL	4.3 (3.2)	0.98	4.0 (4.3)	1.22	0.63	0.22
HadGEM3-GC31-MM	17.1 (13.8)	1.28	0.6 (0.02)	1.05	0.70	0.48
HadGEM3-GC31-HM	19.6 (12.5)	1.39	1.7 (4.0)	1.05	0.64	0.50
HadGEM3-GC31-HH	17.8 (10.7)	1.48	6.5 (7.6)	1.12	0.59	0.36

Formaterad tabell

CMCC-CM2-HR4 **CMCC-CM2-VHR4**	24.4 (21.0) 24.8 (25.6)	1.22 1.34	13.0 (7.8) 15.0 (13.1)	1.22 1.14	0.72 0.59	0.52 0.58
CNRM-CM6.1 **CNRM-CM6.1-HR**	1.09 (0.13) 9.3 (3.2)	1.15 1.18	1.10 (1.30) 2.47 (0.04)	1.07 1.35	0.53 0.48	0.45 0.35
MPI-ESM1-2-HR **MPI-ESM1-2-XR**	10.6 (7.1) 4.6 (0.30)	1.14 0.98	1.2 (0.69) 0.6 (0.47)	1.25 1.16	0.61 0.64	0.44 0.64
AWI-C-1-0-LR **AWI-CM-1-0-HR**	39.5 (24.9) 12.8 (10.1)	no data	20.9 (18.8) 6.1 (4.8)	no data	no data	no data
EC-Earth3P **EC-Earth3P-HR**	0.26 (0.05) 0.95 (0.21)	0.63 1.07	0.24 (0.38) 0.004 (0)	1.02 0.79	0.72 0.50	0.69 0.61

Table 2: Observed and modeled DMV and SHF in the Labrador and Greenland SeaGIN sSeas, their ratio between model and observed values and their correlations between SHF and DMV. Row 2: DMV and SHF in observations, shown are absolute values. Rows 3-9: Ratio of modeled and observed DMV- and SHF (Model values divided through observational values; DMV_{model}/ DMV_{obs} and SHF_{model}/ SHF_{obs}). For ECMWF-IFS, ensemble means are shown. For the DMV (columns 2, 4), the first number compares the mean of the entire historical simulation (1950-2014) to ARGO. The number in brackets only the years 2000-2014. Columns 6, 7: Correlation between winter SHF and March DMV in the respective boxes of the Labrador and Greenland SeaGIN Seas. For the correlations z_{crit0} has been used to avoid complications with periods without any deep convection; the correlations based on $z_{crit1000}$ and $z_{crit700}$ in LAB and GIN Seas are generally similar for models with deep water formation in every winter but much lower in the models with no or very few deep convection events (ECMWF-LR, EC-Earth3P).

Formaterat: Inte Upphöjd/ Nedsän

Formaterat: Inte Upphöjd/ Nedsän

Formaterat: Inte Upphöjd/ Nedsän

Model	**Trend/year historical 1950-2014 DMV-Labrador**	**Trend/year control-1950 year 1-65 DMV-Labrador**	**Trend-difference: hist – control DMV-Lab**	**Trend/year historical 1950-2014 DMV-GINreenland**	**Trend/year control-1950 year 1-65 DMV-GINreenland**	**Trend-difference: hist – control DMV -GIN**
ECMWF-IFS-LR	0.0032.54e+09	-0.01.42e+10	-0.02	0.011.11e+10	0.05e+10	0.06
ECMWF-IFS-MR	-0.54.37e+11	-0.54.37e+11	-3.39	0-5.35e+08	0.0054.83e+09	-0.005
ECMWF-IFS-HR	-3.93e+12 -3.40e+12	-0.43.26e+11	-2.97	0.0021.90e+	0.011.34e+10	-0.012

Formaterat: Teckensnitt:Kursiv

				09		
HadGEM3-GC31-LL	0.41.09e+11	1.58e+12	-1.17	6.62e+12	5.59e+12	1.03
HadGEM3-GC31-MM	***-4.43e+12***	-1.11e+12	*-3.32*	***-1.49e+12***	0.9.73e+11	*-2.46*
HadGEM3-GC31-HM	*-5.133e+12*	*-3.02e+12*	-2.11	***4.40e+12***	-0.33.28e+11	*4.73*
HadGEM3-GC31-HH	***-6.66e+12***	*-2.28e+12*	*-4.38*	0.3.10e+11	-0.95.49e+11	1.25
MPI-ESM1-2-HR	-1.41e+12	-0.62.15e+11	-0.79	-	*-0.8.553e+11*	-0.02
MPI-ESM1-2-XR	***-7.94e+12***	-0.06.02e+10	*-7.88*	*0.82.17e+11* ***-0.41.06e+11***	*0.23.32e+11*	*-0.64*
CMCC-CM2-HR4	***-5.19e+12***	-1.08e+12	*-4.11*	***-9.31e+12***	*-3.97e+12*	*-5.34*
CMCC-CM2-VHR4	-1.42e+12	*-3.27e+12*	1.85	***-1.2.0e+13***	*-2.69e+12*	*-14.69*
CNRM-CM6.1	***-0.54.38e+11***	0.1.62e+11	*-0.70*	*0.8.61e+11*	*0.4.51e+11*	0.41
CNRM-CM6.1-HR	***-6.91e+12***	-0.31.06e+11	*-6.60*	*-1.0.1e+13*	*-1.0.5e+13*	0.4
AWI-CM-1-0-LR	*-1.5.0e+13*	*-1.6.88e+13*	1.80	-1.97e+12	0.6.80e+11	-2.65
AWI-CM-1-0-HR	-0.96.56e+11	-4.98e+12	4.02	1.21e+12	*-2.50e+12*	3.71
EC-Earth3P	0.17.69e+11	0	0.17	***0.43.25e+11***	*0.033.05e+10*	*0.40*
EC-Earth3P-HR	***-0.39.87e+11***	*0.9.22e+11*	*-1.31*	-	0.0033.04e+09	-0.002
				0.0011.39e+09		

Table 3: Trends in the DMV in the Labrador and ~~Greenland Sea~~GIN ~~s~~Seas in the historical simulations and in the first 65 years of the 1950-control simulations (in 10^{12} m^3/year). Trends that are significantly different from 0 at the 95%-confidence level are shown in italic, trends significantly different to the control-runs are bold, and trends significantly different to both 0 and the control-run are italic and bold.

Freshwater fluxes in m^3/s	Fram Strait liquid	Fram Strait solid	Denmark Strait liquid	Denmark Strait solid	North Baffin Bay liquid	North Baffin Bay solid	Sum Fram Strait + Baffin Bay
ECMWF-IFS-LR	12694	154000	60517	92093	21688	7181	195563
ECMWF-IFS-MR	58595	85108	69694	12635	17597	7031	168331
ECMWF-IFS-HR	47578	107470	68940	22533	14479	7367	176894
HadGEM3-GC31-LL	30394	85642	25304	28543	55002	7043	178081
HadGEM3-GC31-MM	81239	82197	69489	21907	19993	6614	190043
HadGEM3-GC31-HM	72294	73470	61834	13905	18728	10309	174801
HadGEM3-GC31-HH	no data	56979	no data	12845	no data	17117	no data
CMCC-CM2-HR4	70915	no data	60545	no data	14854	no data	no data
CMCC-CM2-VHR4	61063	no data	13785	no data	6239	no data	no data
CNRM-CM6.1	39699	43906	33344	8689	35078	3902	122585
CNRM-CM6.1-HR	52321	29243	41327	15409	22297	8540	112401
MPI-ESM1-2-HR	66843	54540	92680	8453	1276	2232	124891
MPI-ESM1-2-XR	54834	62348	112003	12408	2231	3145	122558
EC-Earth3P	26843	96230	30439	28277	25317	5813	154203

Formaterat: Teckensnitt:Inte Kursi
Formaterat: Teckensnitt:Inte Kursi
Formaterat: Teckensnitt:Kursiv
Formaterat: Teckensnitt:Inte Kursi
Formaterat: Teckensnitt:Inte Kursi
Formaterat: Svenska (Sverige)
Formaterat: Teckensnitt:Inte Kursi
Formaterat: Teckensnitt:Inte Kursi
Formaterat: Teckensnitt:Kursiv
Formaterat: Teckensnitt:Inte Kursi
Formaterat: Teckensnitt:Inte Fet, Inte Kursiv
Formaterat: Teckensnitt:Inte Kursi
Formaterat: Teckensnitt:Inte Kursi
Formaterat: Teckensnitt:Inte Kursi
Formaterat: Teckensnitt:Kursiv
Formaterat: Teckensnitt:Inte Fet
Formaterat: Teckensnitt:Inte Kursi
Formaterat: Upphöjd
Formaterat: Upphöjd

EC-Earth3P-HR	22096	105890	54655	27370	1776	3488	133250

Table 4: Liquid and solid freshwater fluxes through Fram Strait, Denmark Strait and northern Baffin Bay in the historical simulations averaged over 1950-2014. Positive values mean freshwater exports out of the Arctic. The last column shows the sum of liquid and solid exports through Fram Strait and Baffin Bay. No data were available to calculate transports in the AWI-CM-1.0 model, liquid freshwater transports in HadGEM3-GC3-HH and sea ice transports in the CMCC-simulations.

Formaterat: Teckensnitt:Inte Fet

Formaterat: Teckensnitt:Inte Fet

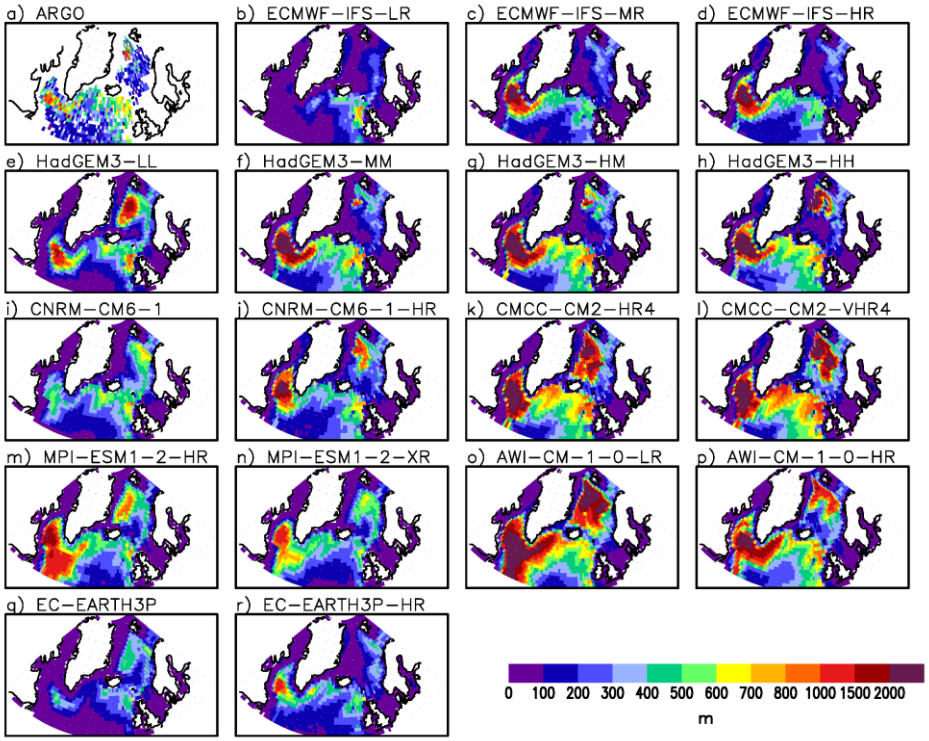

Figure 1: Mixed layer depth in March in the ARGO-data, averaged over 2000-2015 (a) and in the historical low and high-resolution model simulations, averaged over 1950-2014 (b-r).

940

945

950

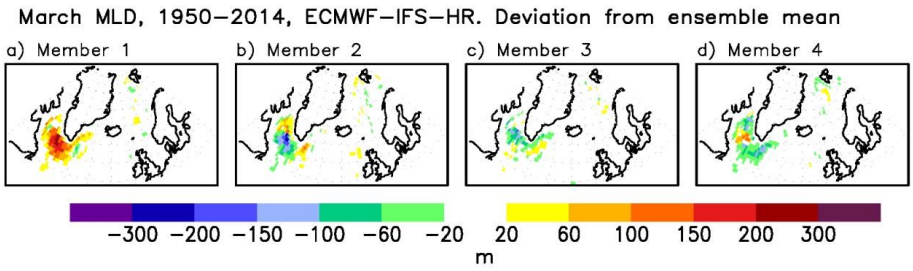

e) DMV in the Labrador Sea in ECMWF-IFS-HR

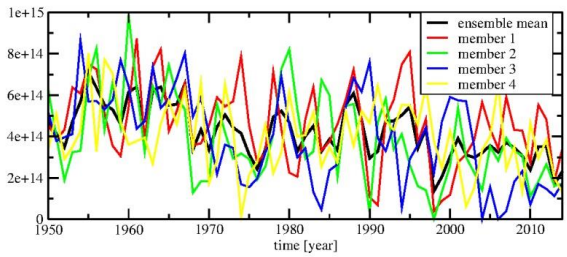

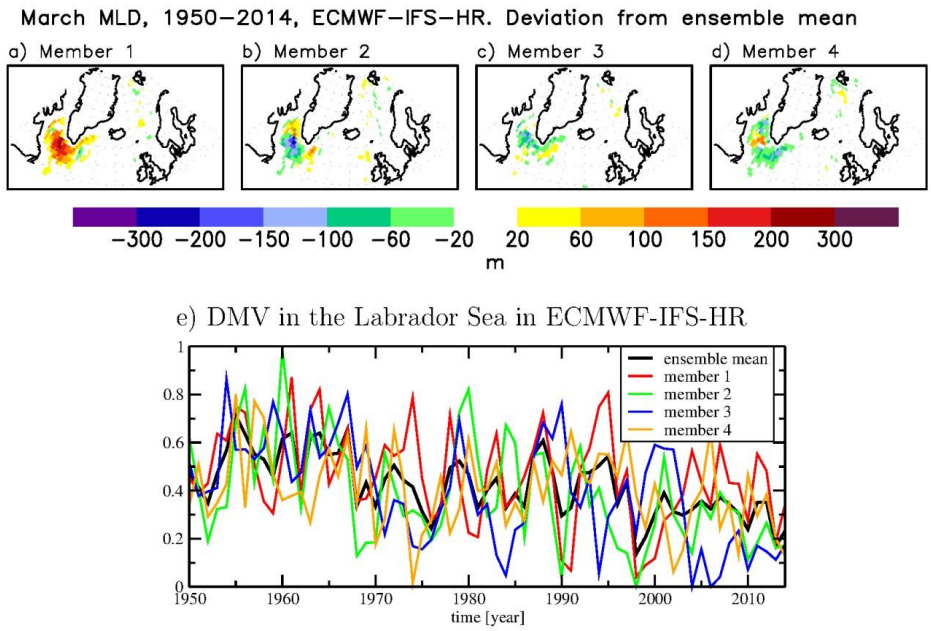

Figure 2: a-d) Deviation of mixed layer depth in March in the ensemble members of ECMWF-IFS-HR from the ensemble mean of the four ECMWF-IFS-HR simulations for the time period 1950-2014. e) DMV in the Labrador Sea (in 10^{15} m^3) in the ensemble mean and single ensemble members of ECMWF-IFS-HR.

Formaterat: Upphöjd

Formaterat: Upphöjd

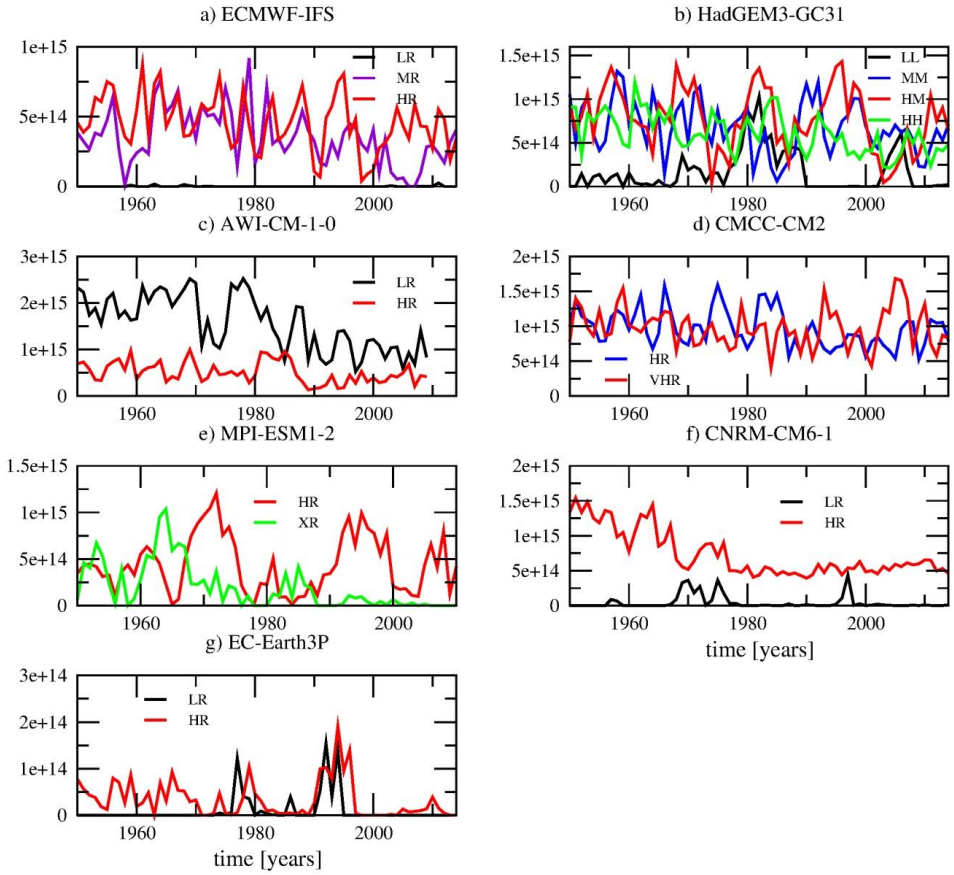
a) ECMWF-IFS
LR
MR
HR
1e+15
5e+14
0
1960
1980
2000
b) HadGEM3-GC31
LL
MM
HM
HH
1.5e+15
1e+15
5e+14
0
1960
1980
2000
c) AWI-CM-1-0
LR
HR
3e+15
2e+15
1e+15
0
1960
1980
2000
d) CMCC-CM2
HR
VHR
2e+15
1.5e+15
1e+15
5e+14
0
1960
1980
2000
e) MPI-ESM1-2
HR
XR
1.5e+15
1e+15
5e+14
0
1960
1980
2000
f) CNRM-CM6-1
LR
HR
2e+15
1.5e+15
1e+15
5e+14
0
1960
1980
2000
time [years]
g) EC-Earth3P
LR
HR
3e+14
2e+14
1e+14
0
1960
1980
2000
time [years]

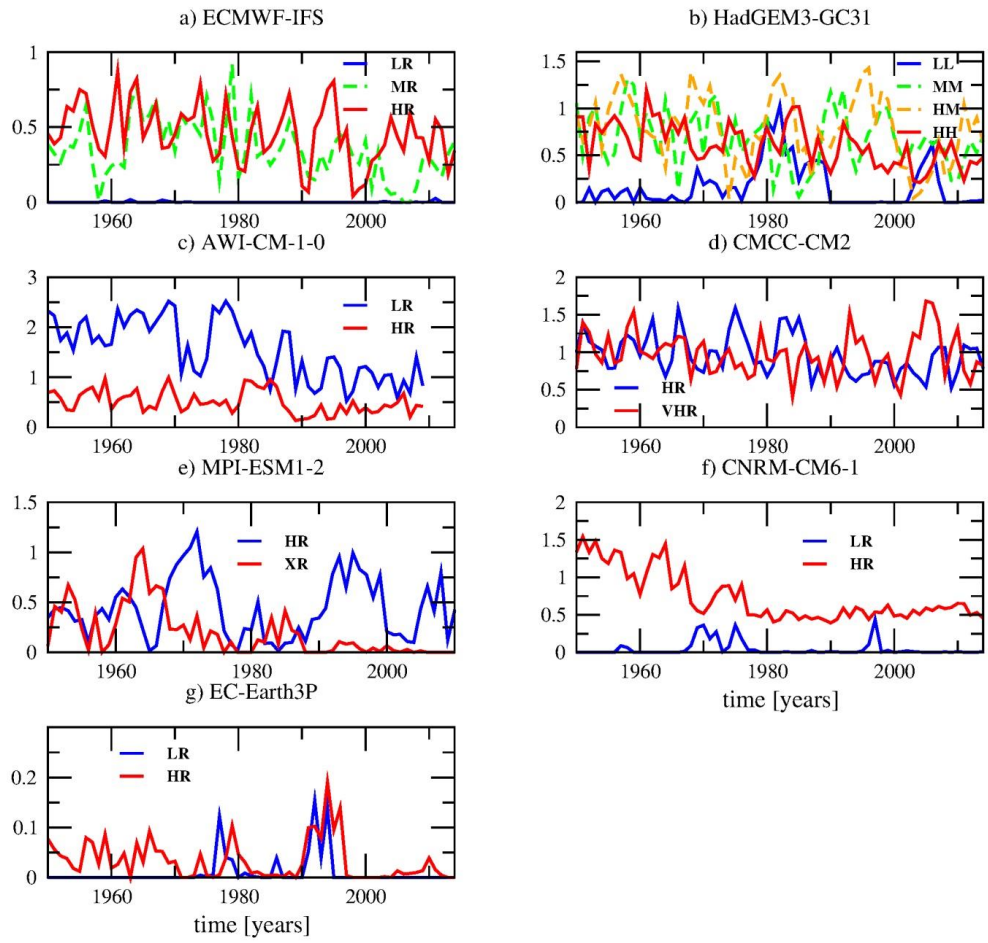

Figure 3: Deep Mixed Volume (DMV) in 10^{15} m^3 using a critical depth of 1000 m in the Labrador Sea in March between 1950-2014. Note the different y-axis between models. For ECMWF-IFS, only member 1 is shown for better visual comparison of the variability across resolutions.

Formaterat: Upphöjd

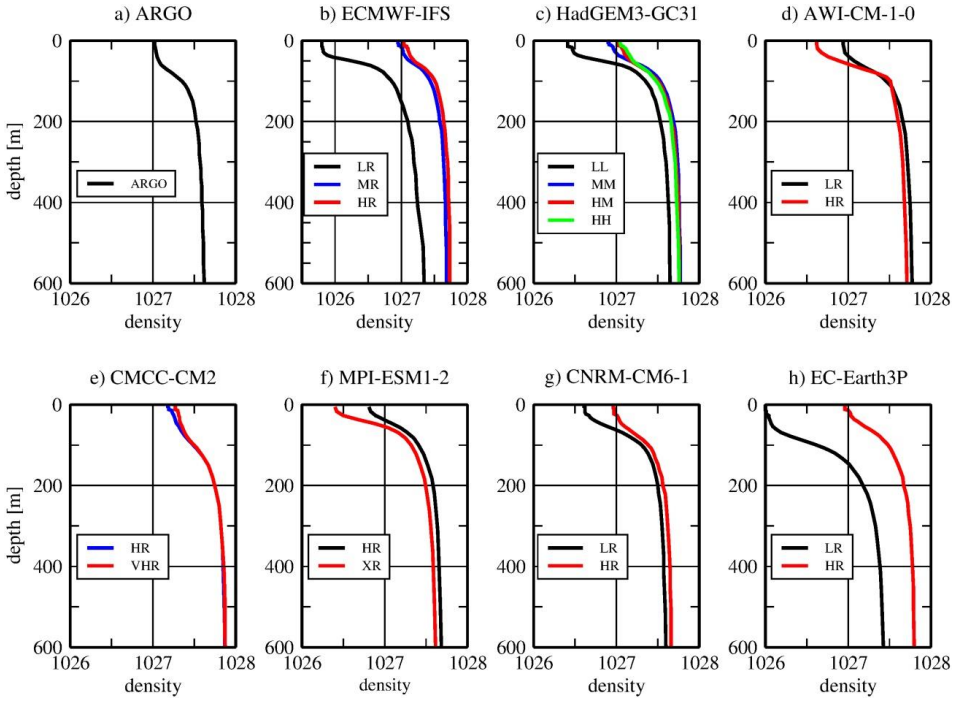
a) ARGO
b) ECMWF-IFS
c) HadGEM3-GC31
d) AWI-CM-1-0
e) CMCC-CM2
f) MPI-ESM1-2
g) CNRM-CM6-1
h) EC-Earth3P
depth [m]
density
0
200
400
600
1026
1027
1028
ARGO
LR
MR
HR
LL
MM
HM
HH
VHR
XR

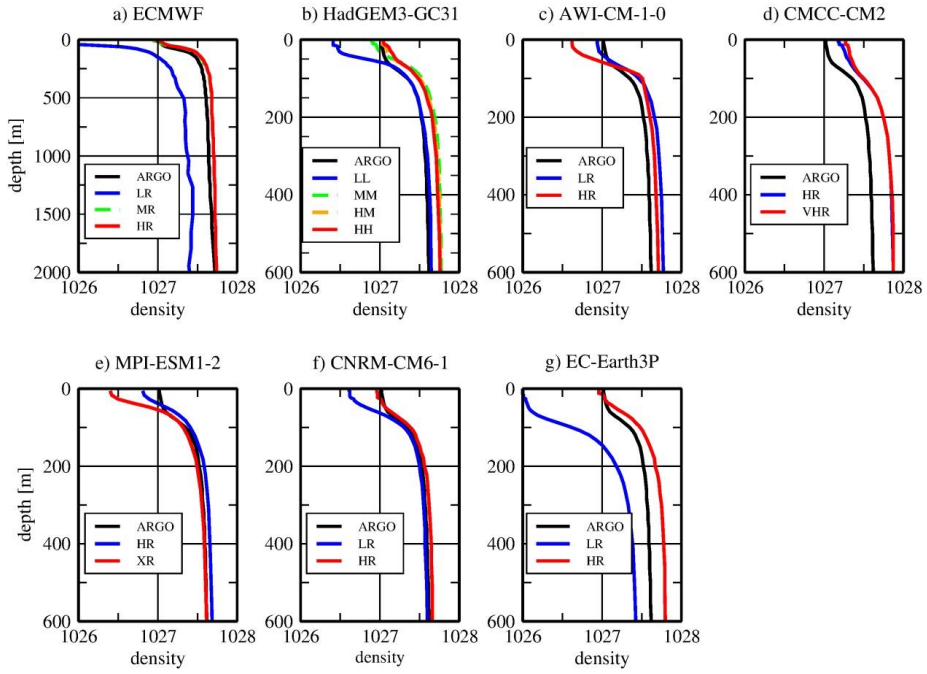

Figure 4: Density (in kg/m^3) in the upper 600 m averaged over the Labrador Sea in November. ~~**Note that the scale of the x-axis differs in b) to capture the low densities of ECMWF-IFS-LR near the surface.**~~

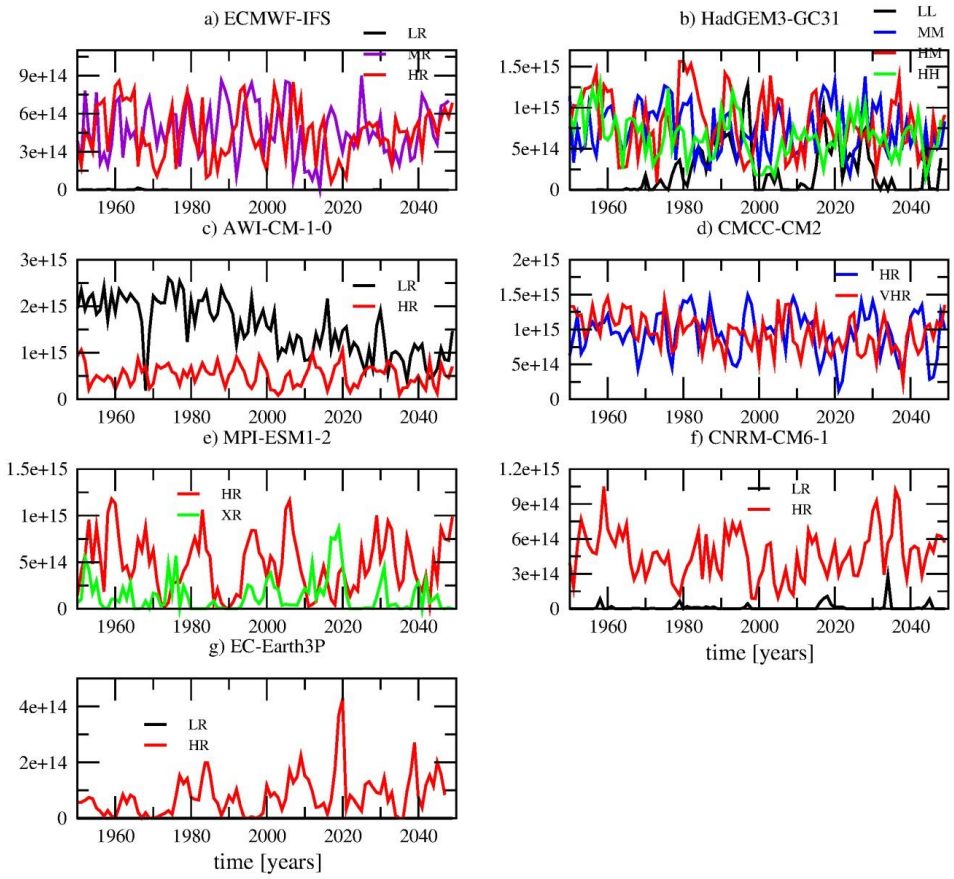
a) ECMWF-IFS
LR
MR
HR
9e+14
6e+14
3e+14
0
1960
1980
2000
2020
2040
b) HadGEM3-GC31
LL
MM
HM
HH
1.5e+15
1e+15
5e+14
c) AWI-CM-1-0
3e+15
2e+15
d) CMCC-CM2
HR
VHR
e) MPI-ESM1-2
f) CNRM-CM6-1
2e+15
1.5e+15
g) EC-Earth3P
XR
1.2e+15
time [years]
4e+14
2e+14

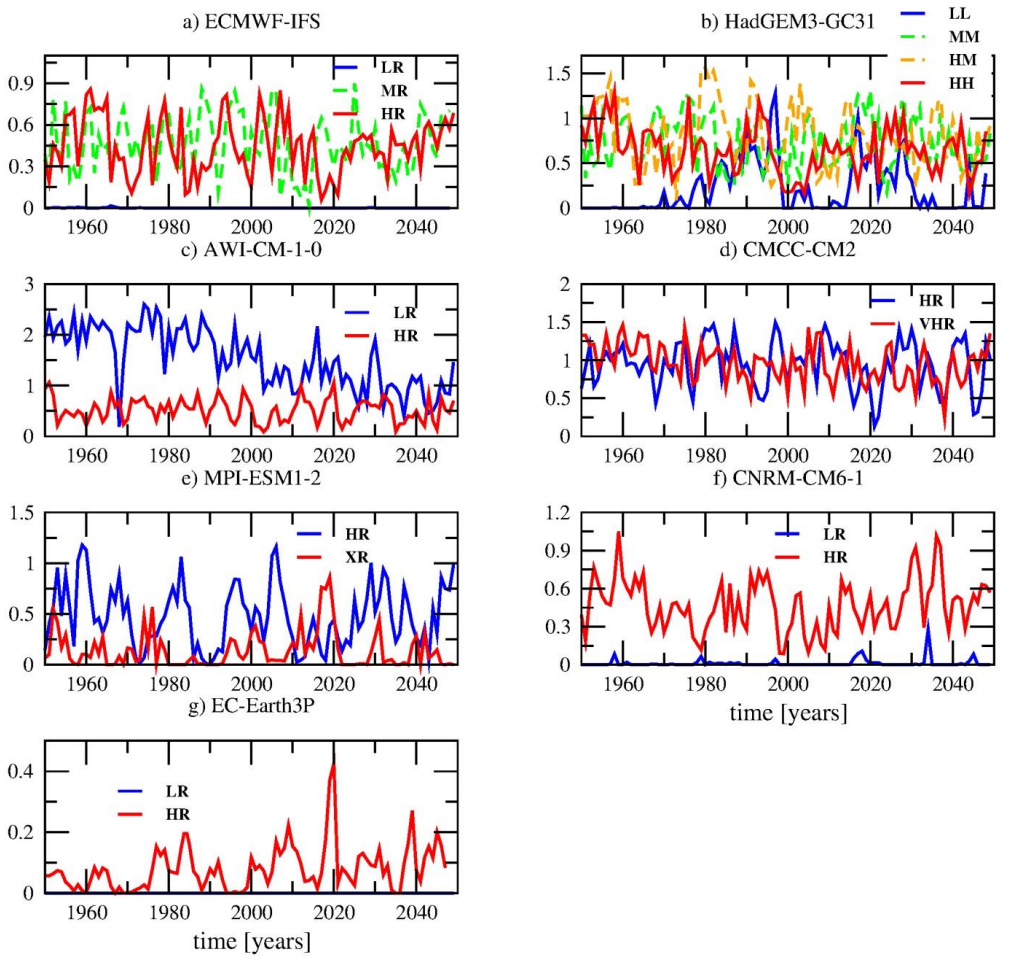

Figure 5: As Figure 3 but for the 100-year control simulation.

1000

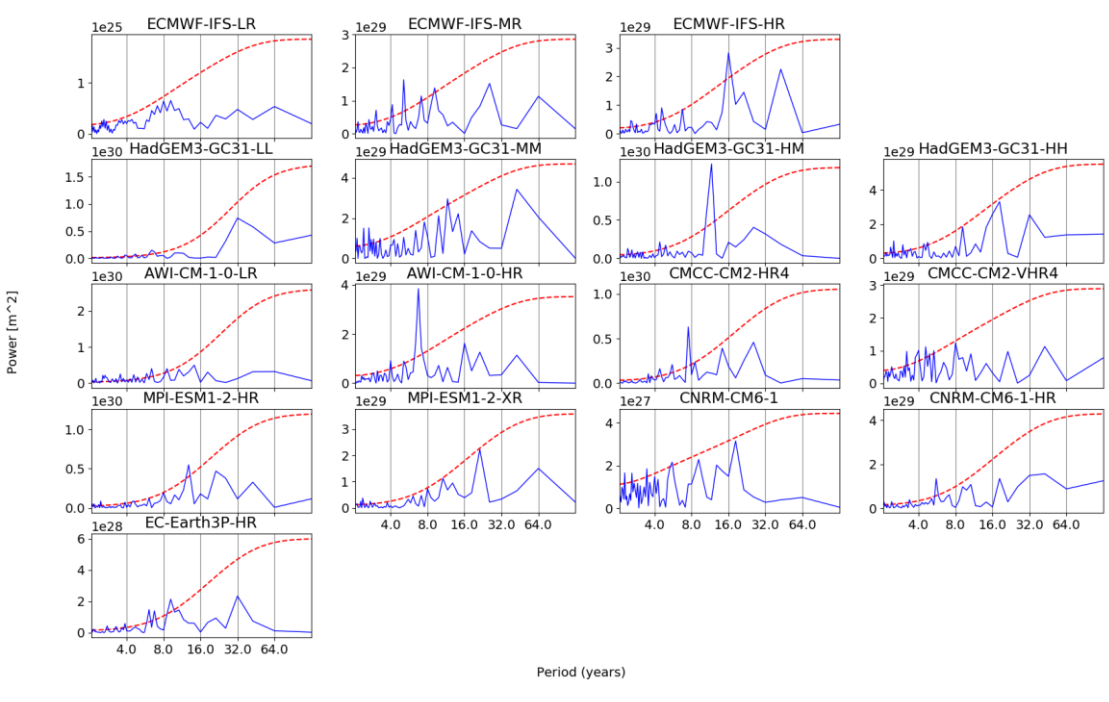
ECMWF-IFS-LR
ECMWF-IFS-MR
ECMWF-IFS-HR
HadGEM3-GC31-LL
HadGEM3-GC31-MM
HadGEM3-GC31-HM
HadGEM3-GC31-HH
AWI-CM-1-0-LR
AWI-CM-1-0-HR
CMCC-CM2-HR4
CMCC-CM2-VHR4
MPI-ESM1-2-HR
MPI-ESM1-2-XR
CNRM-CM6-1
CNRM-CM6-1-HR
EC-Earth3P-HR
Power [m^2]
Period (years)
4.0
8.0
16.0
32.0
64.0

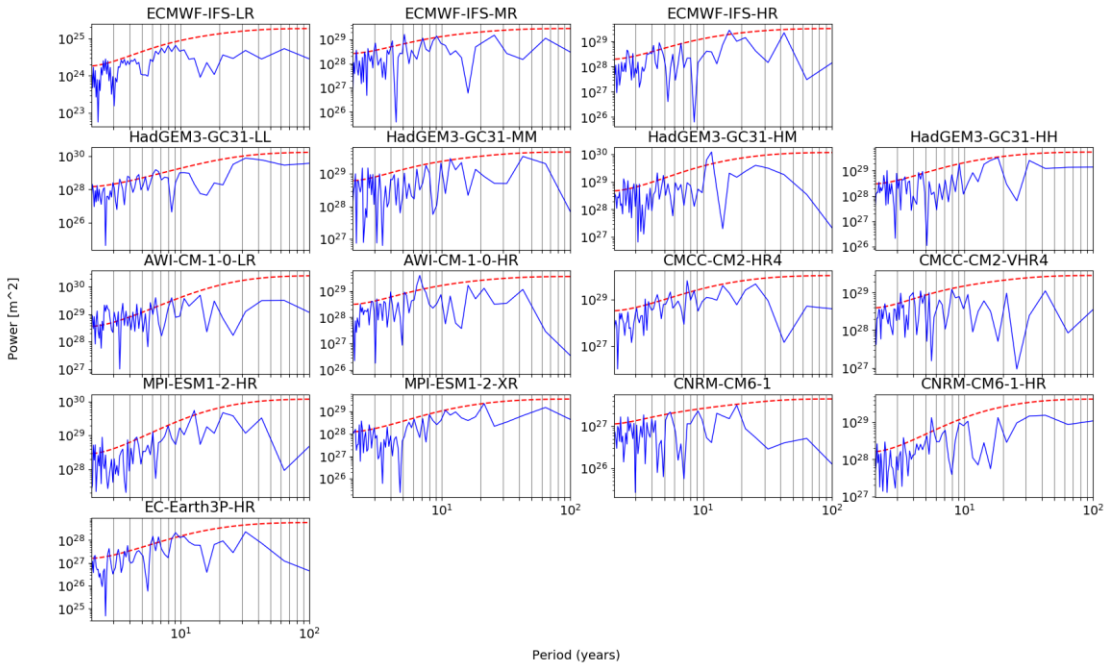

Figure 6: Power spectrum of detrended and normalized March DMV time series of the 100-year control simulation in the Labrador Sea. The dashed red line shows the 95% significance level. The y-axis uses a different scale depending on the model. Note, that no deep convection occurred in the 100-year period in EC-Earth3P.

Formaterat: Teckensnitt:Inte Fet

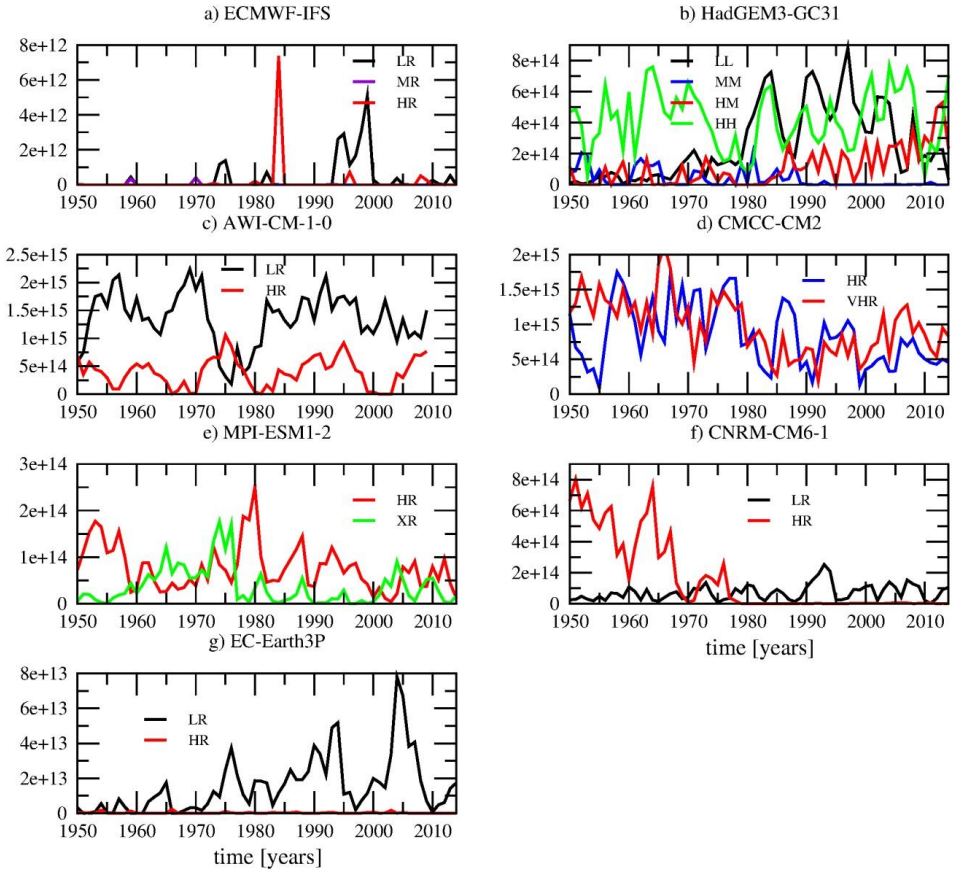
a) ECMWF-IFS
LR
MR
HR
b) HadGEM3-GC31
LL
MM
HM
HH
c) AWI-CM-1-0
LR
HR
d) CMCC-CM2
HR
VHR
e) MPI-ESM1-2
HR
XR
f) CNRM-CM6-1
LR
HR
g) EC-Earth3P
LR
HR
time [years]
1950
1960
1970
1980
1990
2000
2010

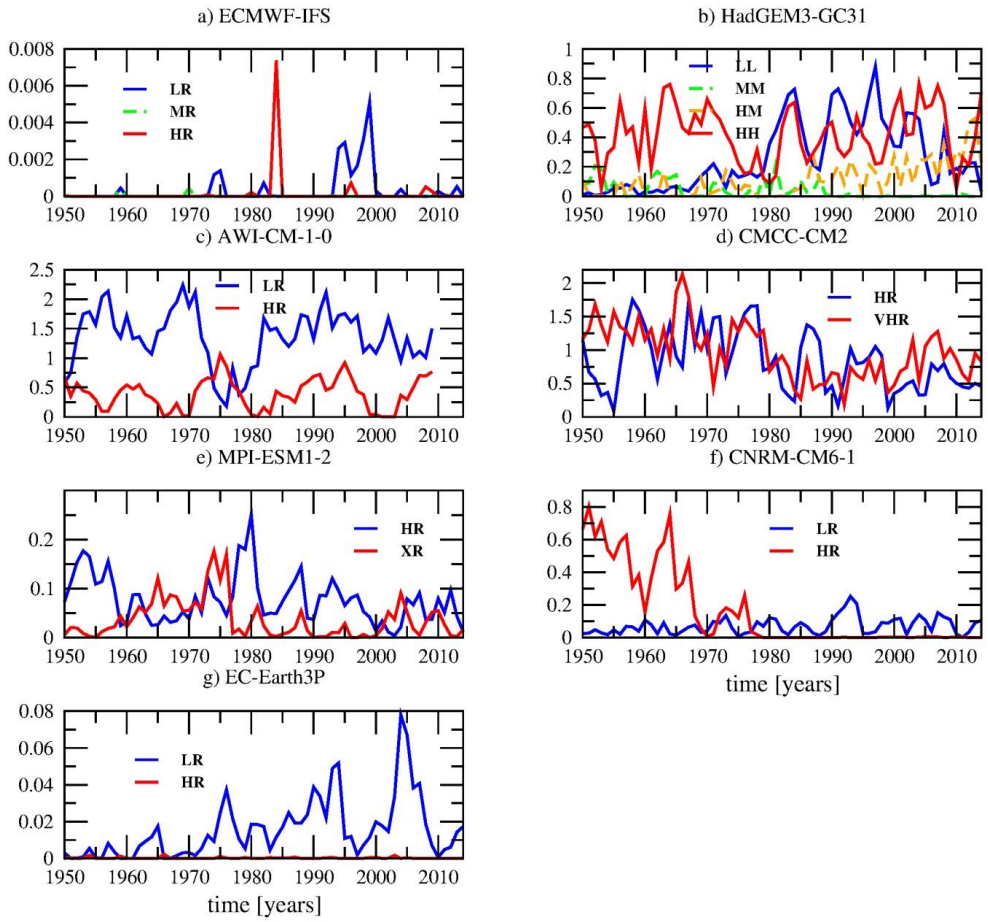

Figure 7: As Figure 3 but for the ~~Greenland Sea~~GIN Seas and a critical depth of 700 m.

1030

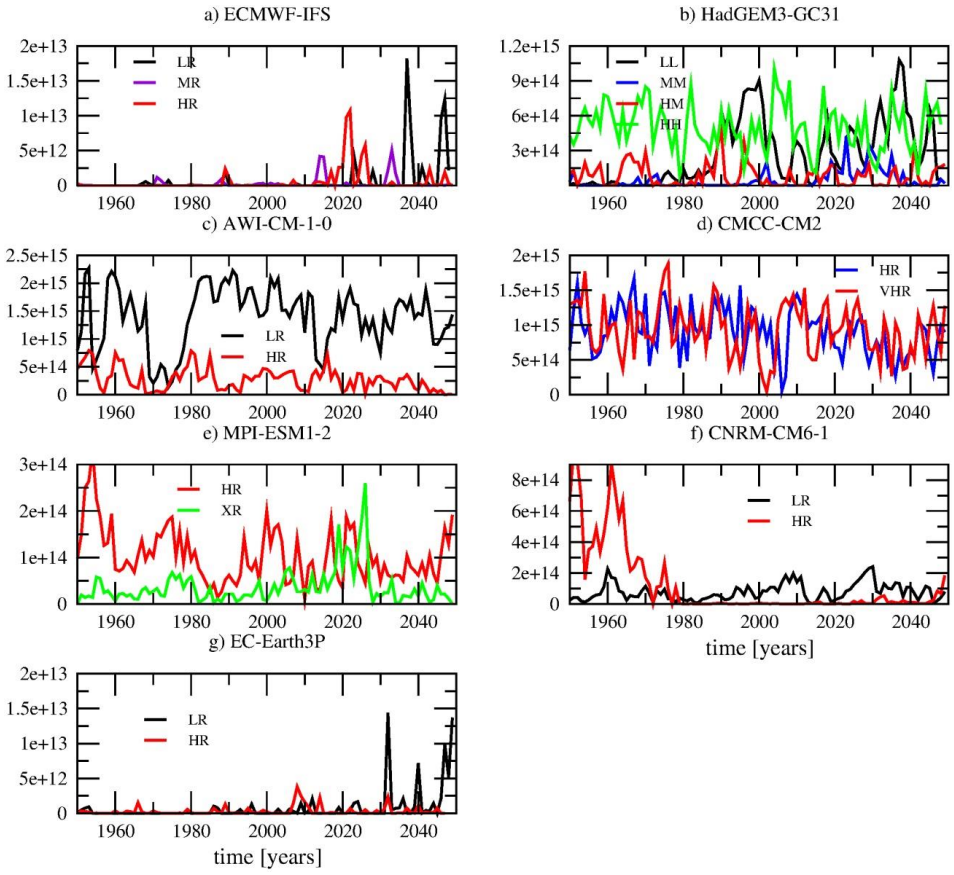
a) ECMWF-IFS
LR
MR
HR
b) HadGEM3-GC31
LL
MM
HM
HH
c) AWI-CM-1-0
LR
HR
d) CMCC-CM2
HR
VHR
e) MPI-ESM1-2
LR
HR
f) CNRM-CM6-1
LR
HR
g) EC-Earth3P
HR
XR
LR
HR
time [years]
1960
1980
2000
2020
2040

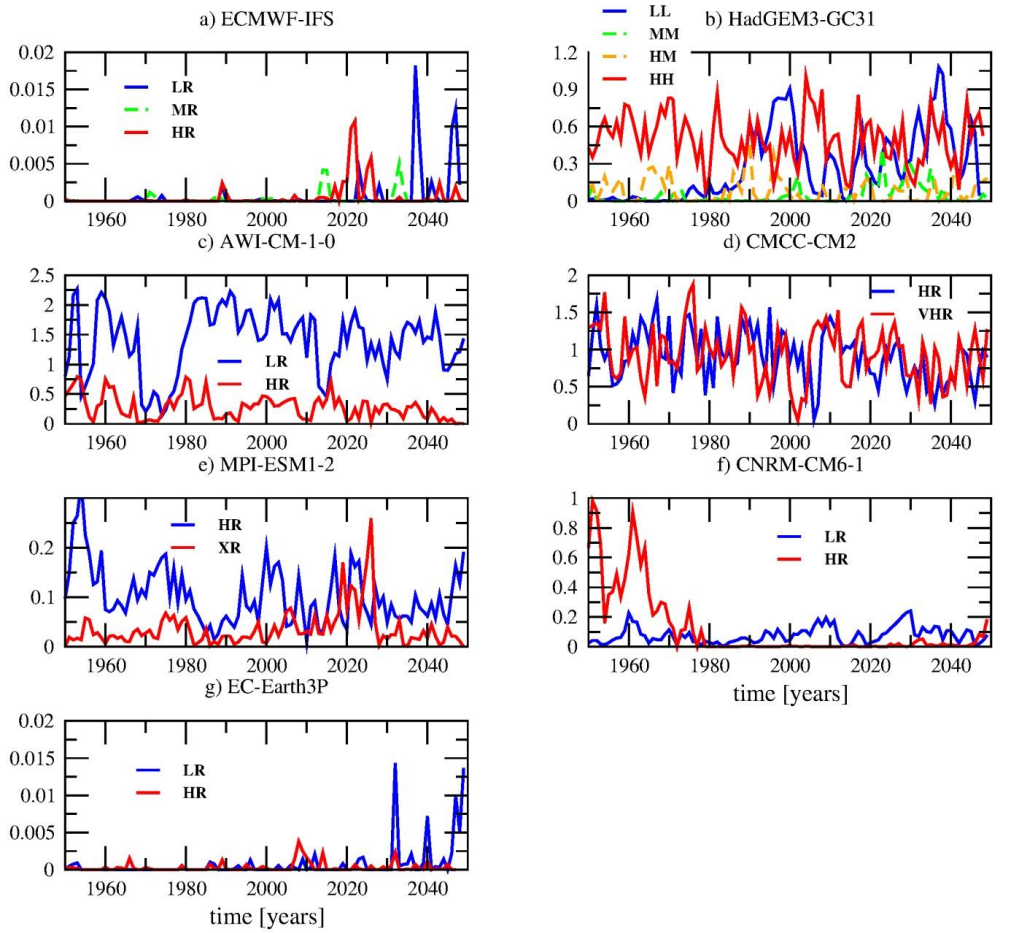

Figure 8: As Figure 7 but for the 100-year 1950-control simulations.

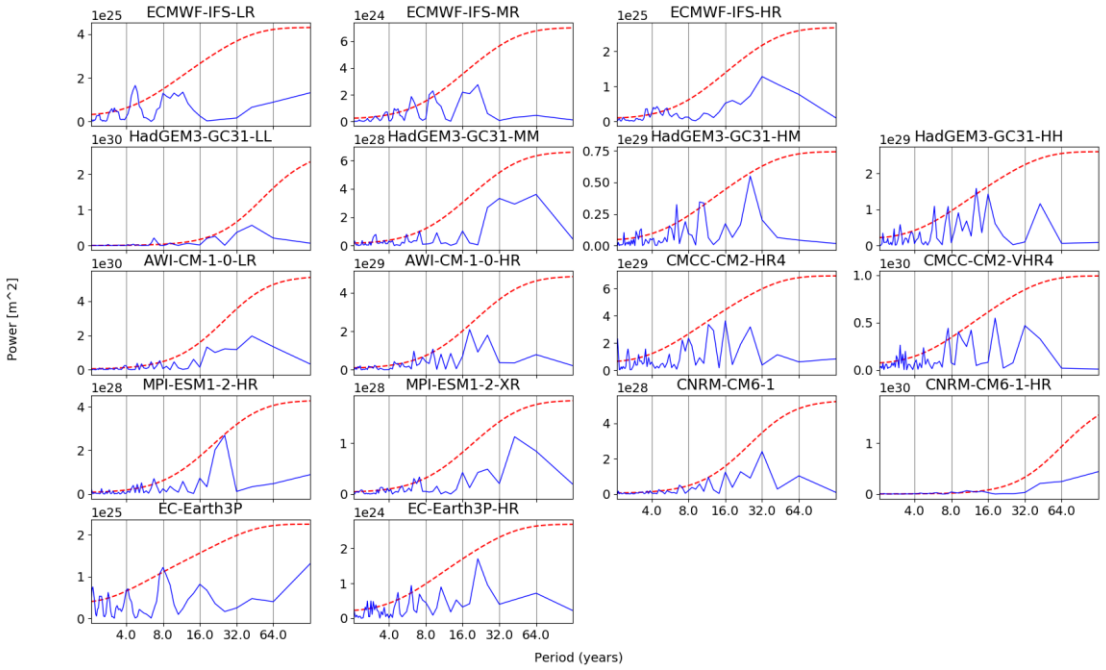
ECMWF-IFS-LR
ECMWF-IFS-MR
ECMWF-IFS-HR
HadGEM3-GC31-LL
HadGEM3-GC31-MM
HadGEM3-GC31-HM
HadGEM3-GC31-HH
AWI-CM-1-0-LR
AWI-CM-1-0-HR
CMCC-CM2-HR4
CMCC-CM2-VHR4
MPI-ESM1-2-HR
MPI-ESM1-2-XR
CNRM-CM6-1
CNRM-CM6-1-HR
EC-Earth3P
EC-Earth3P-HR
Power [m^2]
Period (years)
4.0
8.0
16.0
32.0
64.0

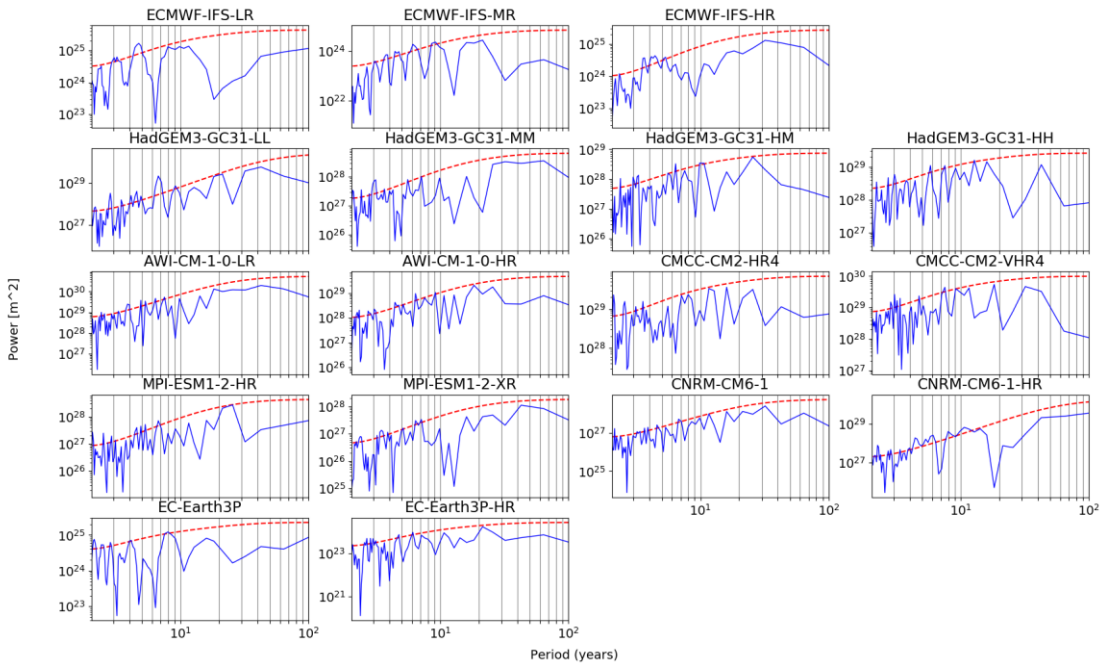

Figure 9: Same as Figure 6 but for DMV in the ~~Greenland Sea~~GIN Seas.

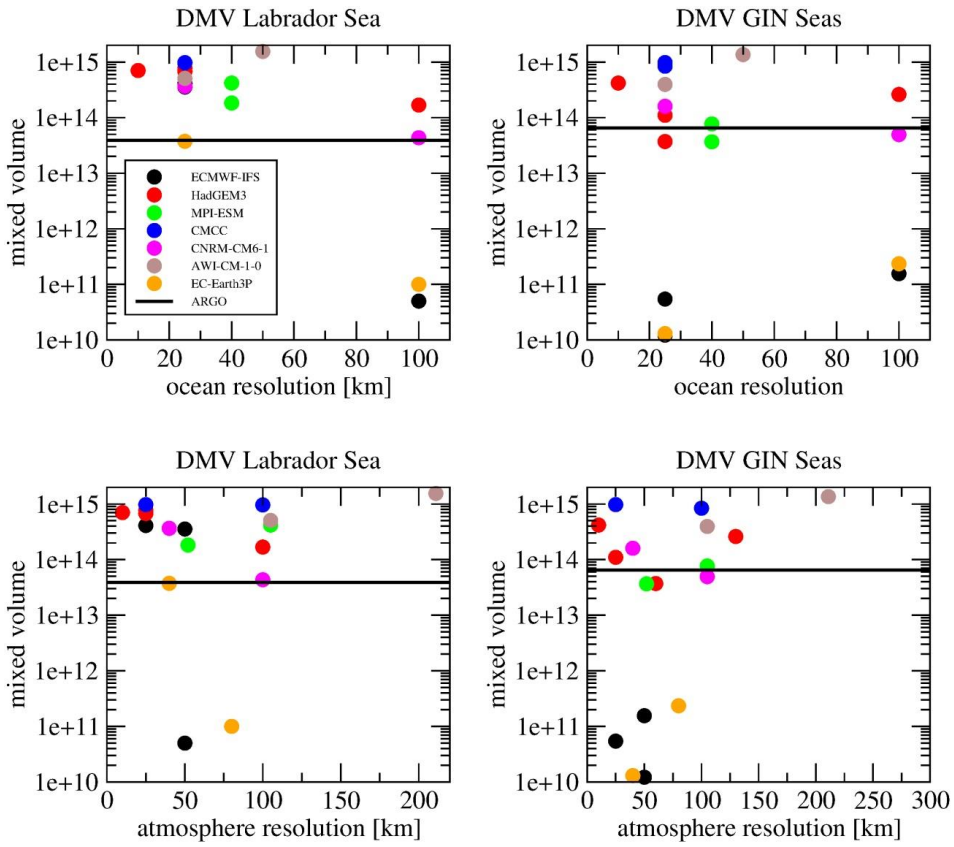
DMV Labrador Sea
DMV GIN Seas
mixed volume
1e+15
1e+14
1e+13
1e+12
1e+11
1e+10
0
20
40
60
80
100
ocean resolution [km]
ocean resolution
ECMWF-IFS
HadGEM3
MPI-ESM
CMCC
CNRM-CM6-1
AWI-CM-1-0
EC-Earth3P
ARGO
50
150
200
250
300
atmosphere resolution [km]

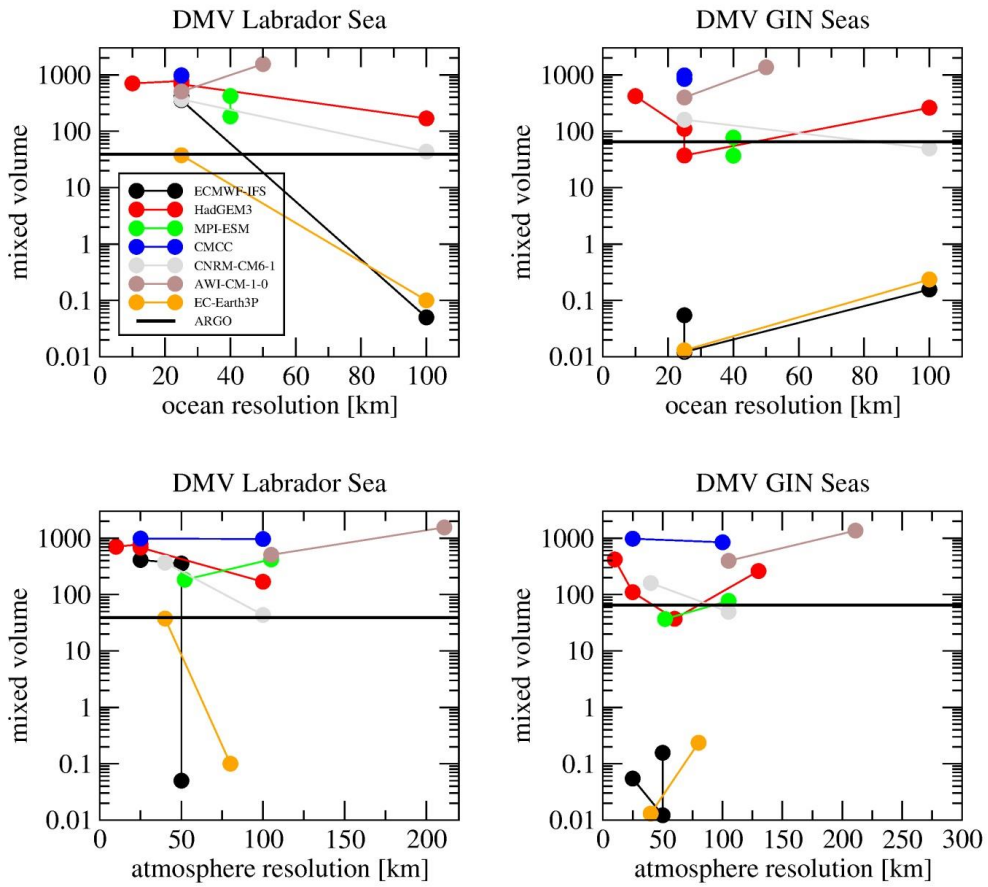

Figure 10: DMV (average over 1950-2014 in 10^{12} m^3) in Labrador Sea (left) and GIN-Seas (right) in March in dependence on the oceanic (top) and atmospheric (bottom) resolution. Thin lines connect model versions with different resolution of the same model.~~Average over 1950-2014.~~

Formaterat: Upphöjd

1070

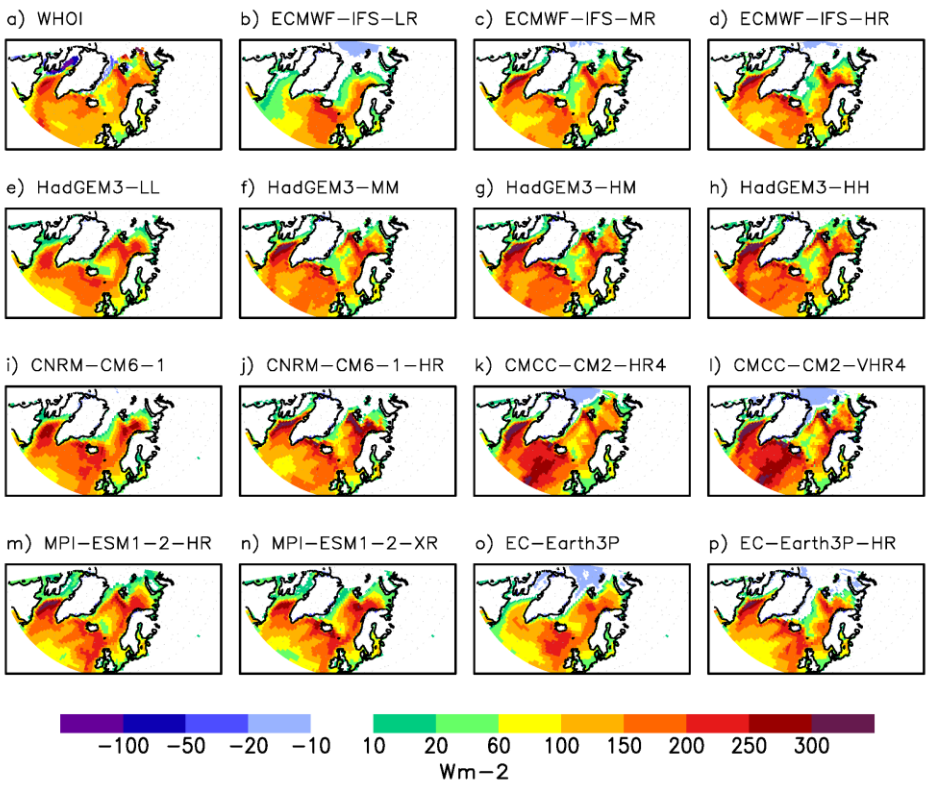
a) WHOI
b) ECMWF−IFS−LR
c) ECMWF−IFS−MR
d) ECMWF−IFS−HR
e) HadGEM3−LL
f) HadGEM3−MM
g) HadGEM3−HM
h) HadGEM3−HH
i) CNRM−CM6−1
j) CNRM−CM6−1−HR
k) CMCC−CM2−HR4
l) CMCC−CM2−VHR4
m) MPI−ESM1−2−HR
n) MPI−ESM1−2−XR
o) EC−Earth3P
p) EC−Earth3P−HR
−100 −50 −20 −10 10 20 60 100 150 200 250 300
Wm−2

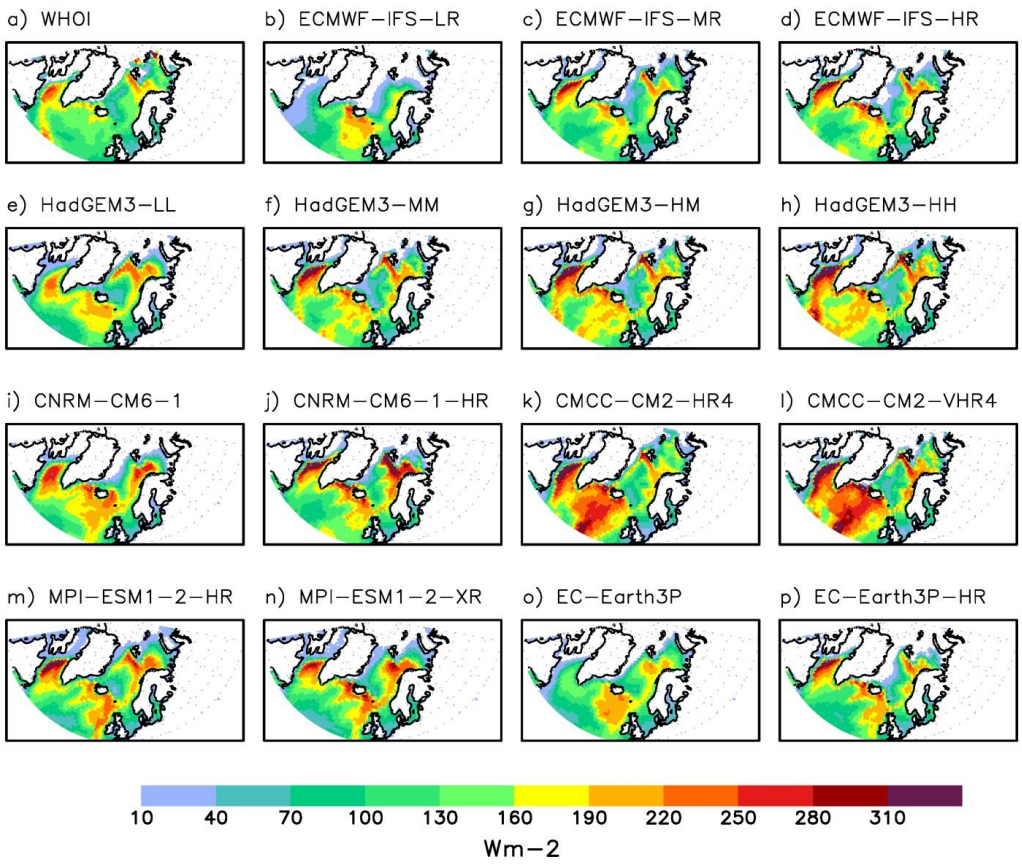

Figure 11: Turbulent surface heat flux (January, February, March average) in 1950-2014 in the WHOI-OAFlux data and in the model simulations. Positive values mean flux from the ocean to the atmosphere.

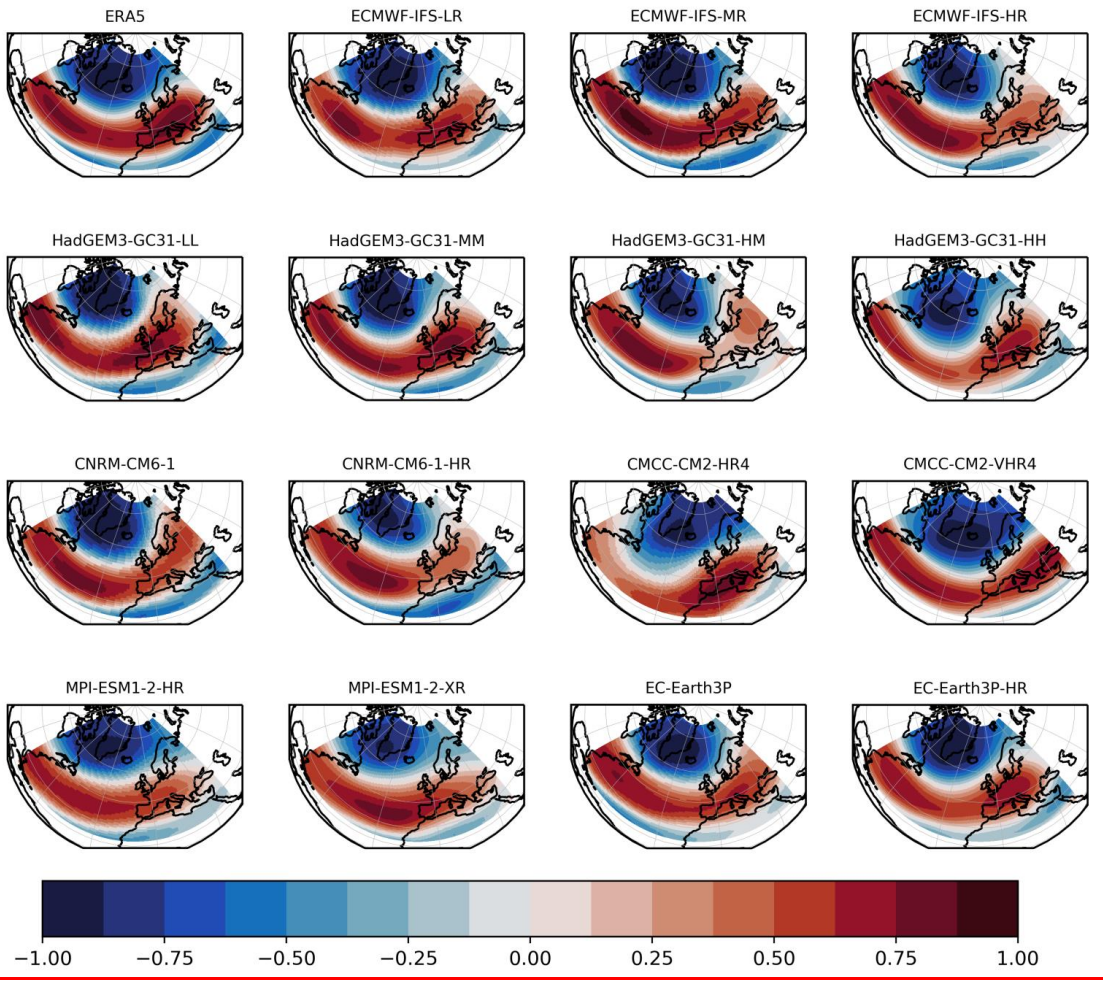

Figure 12: Pearson correlation between geopotential height at 500 hPa and North Atlantic Oscilation (NAO) index during winter (JFM mean) for ERA5 and the models. The periods used were 1979-2019 for ERA5 and 1950-2014 for the models.

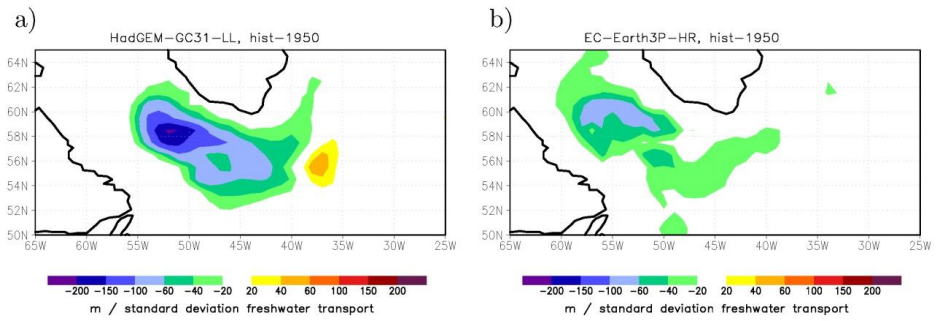

Figure 1~~3~~2: Regression between annual mean freshwater transport through the Denmark Strait and mixed layer depth in the following March. a) HadGEM-CG31-LL and b) EC-Earth3P-HR. Data have been detrended before calculating the regression. These two simulations show the largest correlation between Denmark Strait freshwater transport and DMV in the Labrador Sea (-0.4 and -0.35 for HadGEM-GC31-LL and EC-Earth3P-HR, respectively).

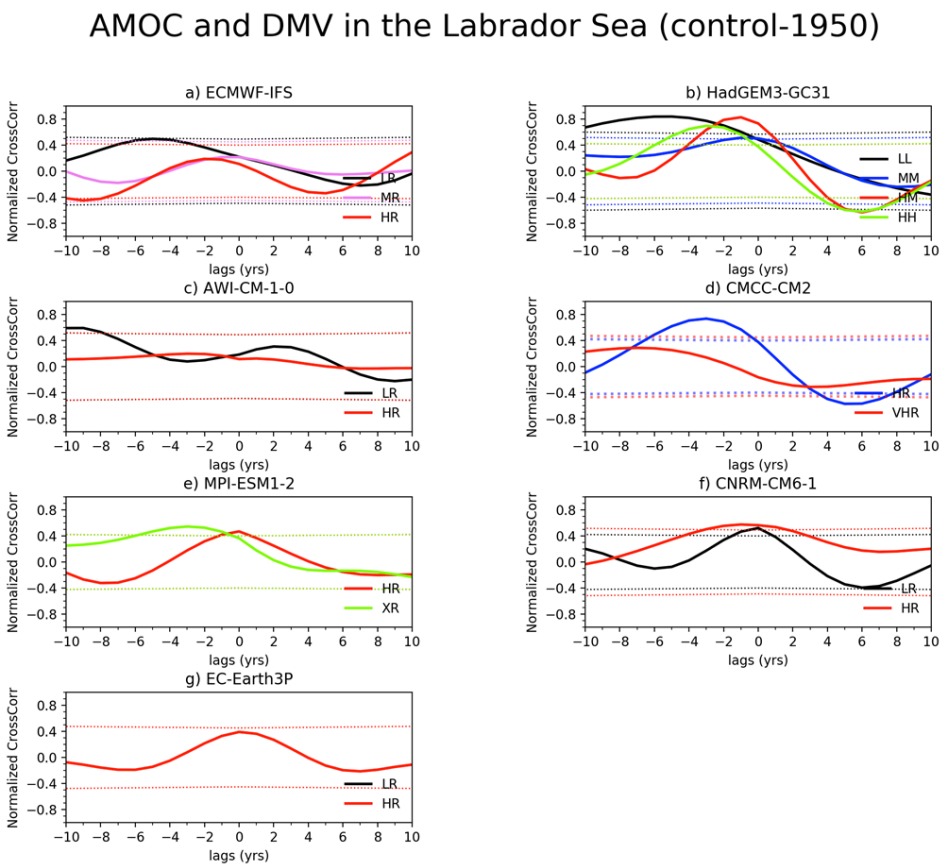
AMOC and DMV in the Labrador Sea (control-1950)
a) ECMWF-IFS
b) HadGEM3-GC31
c) AWI-CM-1-0
d) CMCC-CM2
e) MPI-ESM1-2
f) CNRM-CM6-1
g) EC-Earth3P
Normalized CrossCorr
lags (yrs)
LR
MR
HR
LL
MM
HM
HH
VHR
XR

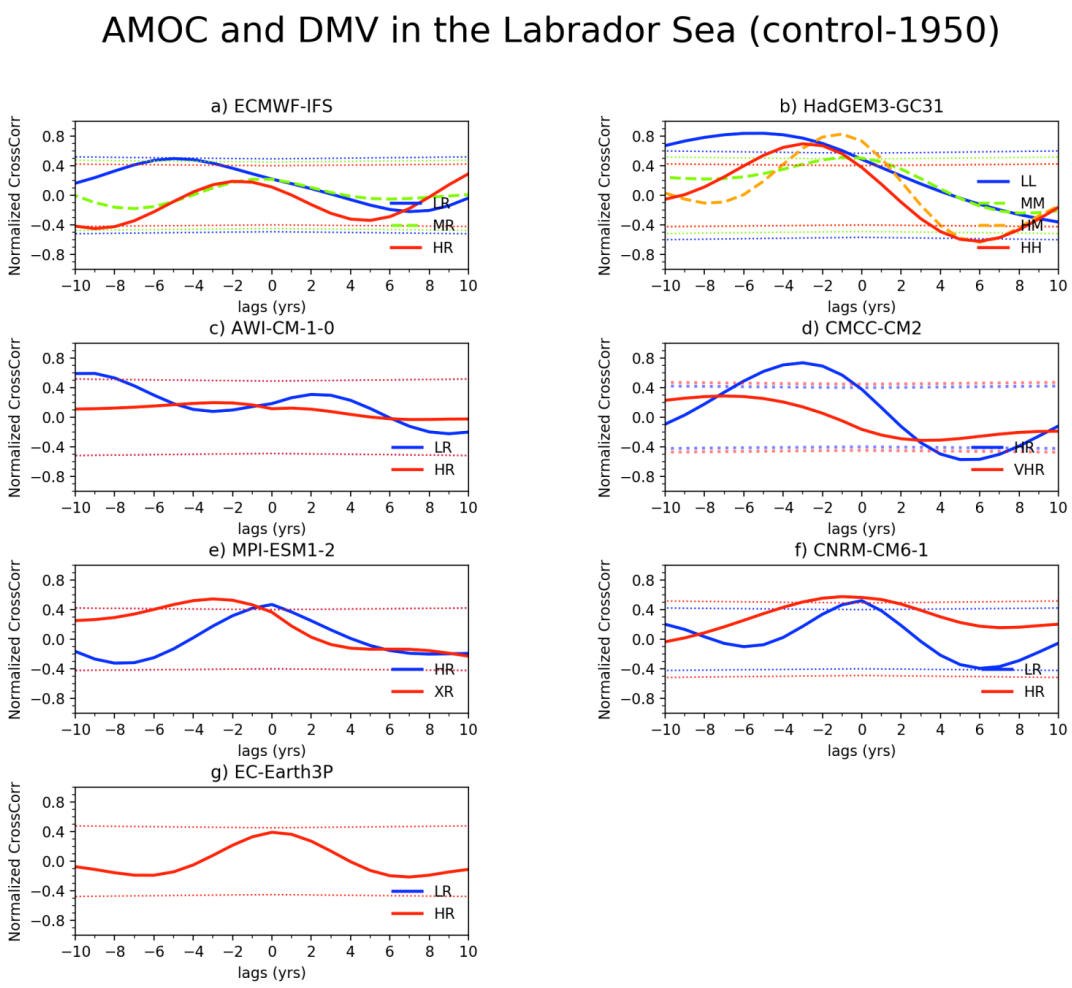

Figure 143: Crosscorrelation between the DMV using a critical depth of 1000 m in the Labrador Sea in March and the AMOC index for the 100-year control simulation. Both timeseries were detrended and filtered with a 10 years low-pass filter. Area enclosed by dotted lines represents the 95% confidence calculated as 2/sqrt(N), where N is the number of independent data based on the time that takes autocorrelation to fall below 1/e. Positive lags mean AMOC leads DMV, negative lags mean DMV leads AMOC. The low resolution version of EC-Earth3P does not produce any deep convection events in the control simulation.

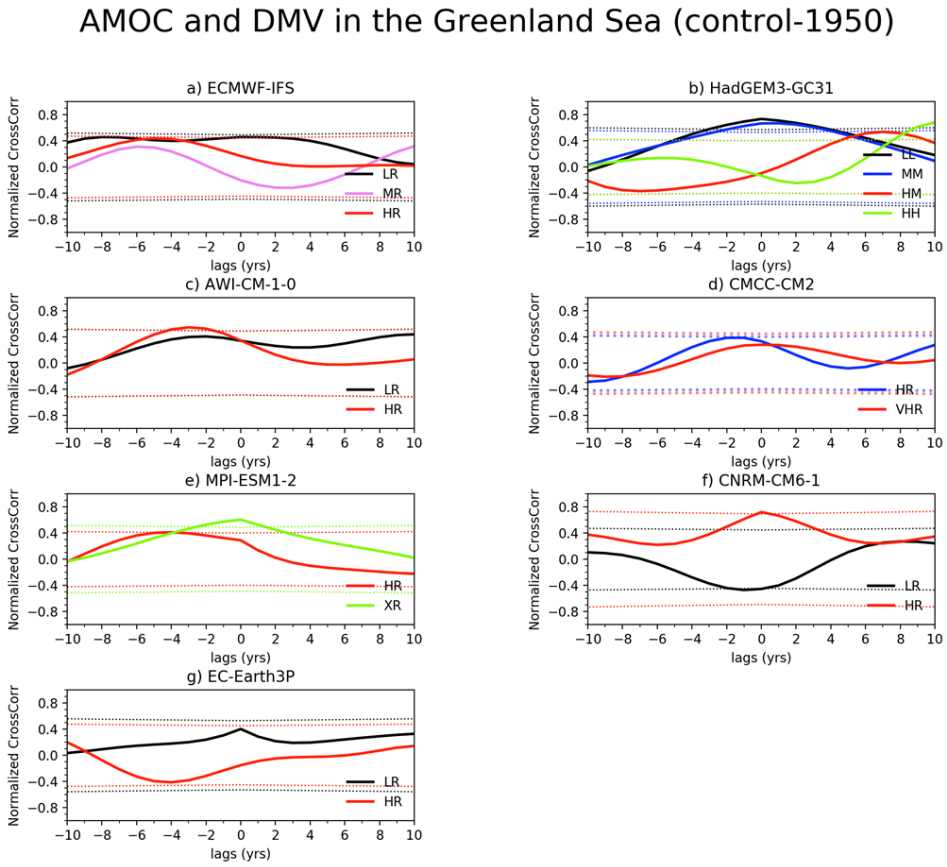
AMOC and DMV in the Greenland Sea (control-1950)
a) ECMWF-IFS
b) HadGEM3-GC31
c) AWI-CM-1-0
d) CMCC-CM2
e) MPI-ESM1-2
f) CNRM-CM6-1
g) EC-Earth3P
Normalized CrossCorr
lags (yrs)
LR
MR
HR
LL
MM
HM
HH
VHR
XR

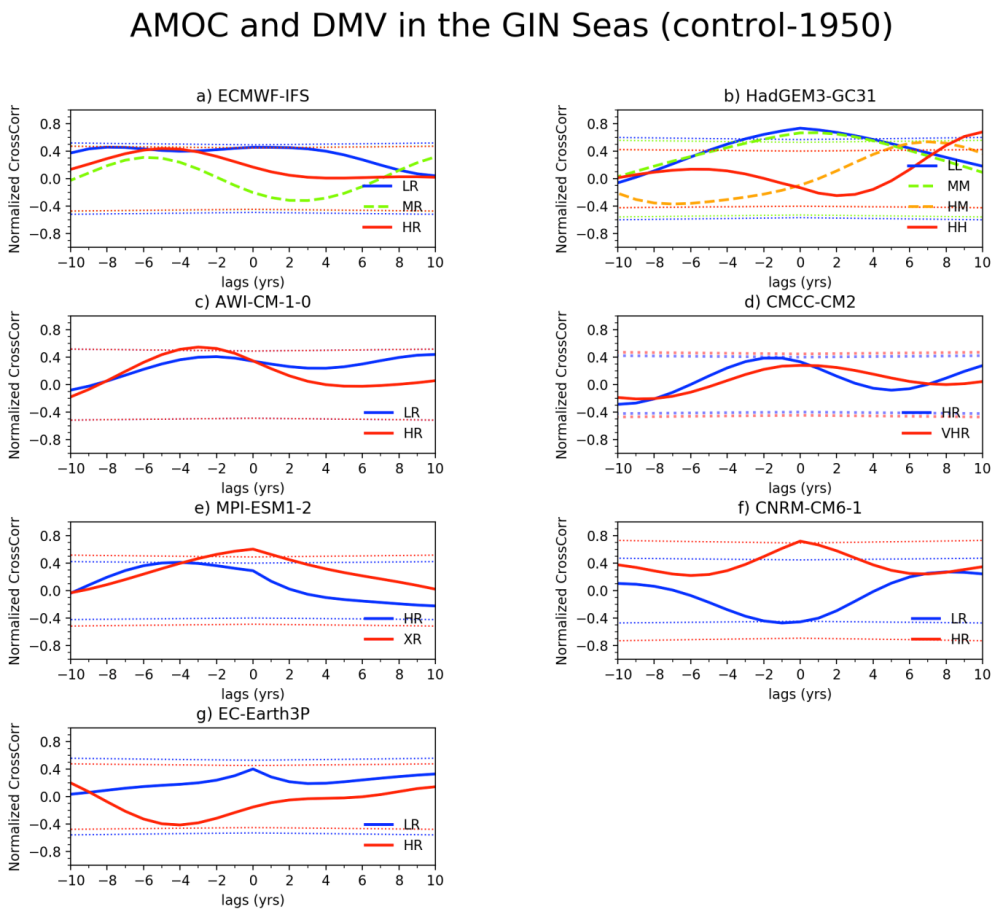

Figure 154: As Figure 12 but for the ~~Greenland Sea~~GIN Seas and a critical depth of 700 m.